Effect of Microstructure on the Performance of Corrosion Resistant Alloys

Marzieh Kishan Roodbari

Preface

This work was carried out at Norsk Hydro, Karmøy, as master thesis in spring 2015. I hereby declare that this work was carried out by me, Marzieh Kishan, according to the regulations at NTNU.

First, I would like to express my gratitude to my supervisor, Prof. Jan Halvor Nordelin, for all his guidance, patience, and assistance. We had so many fruitful discussions during this project, and I learned a lot from him.

I received precious assistance from Dr. Jan Tore Buvik Gundersen, my industrial supervisor. His word always gave me hope and confidence to successfully finish this project. I would like to express my appreciation to Prof. Ann Mari Svensson for helping me to get this industrial thesis and introducing me to Norsk Hydro.

I am greatly indebted to Dr. Esma Senel, for all she has done for me. She is brilliant and incredibly willing to share her knowledge. Her guidance and assistance throughout this project were very helpful. Moreover, I would like to appreciate her for assisting me with practical matters.

I would like to show my appreciation to all employees at the research department in Norsk Hydro, Karmøy, for their fantastic support and understanding.

Stavanger, June 2015   Marzieh Kishan

Dedication

This thesis is dedicated to my husband, Ehsan. I give my deepest expression of love and appreciation for the encouragement that you gave and the sacrifices you made during this Master Program. Thank you for the support and understanding during late nights of typing.

Abstract

Corrosion by pitting in aluminium alloys is a very complex process that can be affected by various factors such as chemical composition and microstructure of the alloys. The electrochemistry and distribution of second phases populating the alloy are the main factors that significantly influence the corrosion of aluminium alloys.

The purpose of the present work is to contribute to a deeper understanding of how the chemical composition and microstructure affect the ability of an aluminium alloy to form a passive layer and its susceptibility to localized corrosion. To carry out the experiment, samples of alloys 3003, 5049, 6061, and 6063 were prepared. The open circuit potential transient technique was utilized to investigate the corrosion potential of alloys under study. The ability of alloys to form the passive layer and the corrosion parameters such as corrosion potential were determined using potentiodynamic polarization measurement.

In this study, the corrosion behaviour of alloys was explored as a function of time using the salt spray test. For each type of alloy, we considered 26 samples, prepared from tubes, and tested in a salt spray chamber in the duration of 49 days. At specified intervals, two samples of each alloy were taken out from the chamber. The type of corrosion and the corrosion rate were investigated through this test. As pitting is the main corrosion process, the depth of ten deepest pits were measured using optical microscopy. Also, the cross section of the deepest pit was analysed to see if the alloy is susceptible to intergranular corrosion.

Statistical analysis was carried out in order to investigate the variation of corrosion rate during exposure and to predict the lifetime of a component. In particular, the Extreme Value theory, the Gumbel distribution, was employed to plot the probability paper of the extreme pit depth occurrence. In addition, the Gumbel distribution theory was utilized to extrapolate data to longer exposure times.

Contents

List of Figures

List of Tables

Chapter 1

Introduction

aluminium and aluminium alloys represent an important category of materials due to their high technological value and wide range of industrial applications, especially in marine applications [1, 2]. aluminium and its alloys are generally passive and corrosion resistant in aqueous solutions except for pitting corrosion due to some reactive species. The surface oxide film on these materials is stable in the pH range 4-9 [1]. Aggressive anions, like chloride ion lead to increased corrosion rates and film breakdown. The effect of alloying elements on the breakdown of the passive film was extensively studied using various grades of aluminium and different metals [3, 4, 5, 6, 7]. It has been established that the presence of alloying elements in the microstructure such as insoluble intermetallic particles or single elements (Cu, Si), leads to formation of local electrochemical cells between them and the aluminium matrix [2, 8, 9]. This causes severe and highly localized attack by pitting in aggressive medium [1, 10]. The electrochemical nature of the intermetallics phases plays a vital role in susceptibility of an Al alloy to localized corrosion.

In regards to the 5xxx series Al-alloys, these alloys are based on additions of magnesium (Mg), along with secondary additions of manganese and often minor levels of chromium [4]. Such alloys are widely employed due to their moderate strength combined with corrosion resistance in marine environments. Al–Mg–Si (6xxx series) alloys are generally considered to have good corrosion resistance compared to Cu or Zn rich high strength Al-alloys that are highly suitable in various marine applications. aluminium alloys of 3xxx series, due to their favorable strength-to-weight property as well as good corrosion resistance, have been widely used in many application. However these alloys are also susceptible to localized corrosion; pitting and intergranular corrosion. These types of alloys are used in a huge number of applications that aggressive ions may be presence and attack the protective film. As a consequence, localized corrosion, specially pitting corrosion, cause failure in whole component just for a small and shallow pit. The kind and amount of alloying elements that add to generate high strength alloys have a significant influence on susceptibility of these alloys to localized corrosion.

Localized forms of corrosion, such as pitting corrosion, are difficult to quantify and model because the corrosion rate at a particular location on a sample depends sensitively on the many local microscopic material and environmental conditions [11]. As a result, at a macroscopic level, pitting corrosion often appear to occur in a random, probabilistic manner. Statistical approaches have been used to quantify and model localized corrosion without requirement to microscopic characterization of whole structure in all periods. In particular, the theory of extreme value analysis [11, 12, 13] has been successfully applied to pitting corrosion in aluminium [14]. Extreme value analysis enables prediction of the most probable maximum extent of corrosion, for example, the deepest pit in the case of pitting corrosion. Extreme value analysis is, therefore, well suited to localized corrosion because failure induced by localized corrosion usually occurs when any local site fails [15].

1.1 Objective and approach

Due to applications of aluminium alloys to marine environment, it is necessary to study the factors affected localized corrosion susceptibility. In addition, pit development during time can give useful and valuable information that helps to predict the lifetime of a component. This work will focus on corrosion behaviour of alloys 3003, 5049, 6061, and 6063 using electrochemical measurements and salt spray test combine with statistical analysis of maximum pit depths in order to study the influence of alloying elements and microstructure on corrosion of aluminium alloys.

The main objective of this project is to investigate how different alloying elements affect the susceptibility of aluminium alloys to pitting and intergranular corrosion in aggressive environments.

The present project is also concerned with the development with time of maximum pit depth and its variability for pitting corrosion along tubes made from different aluminium alloys expose to acidified seawater. statistical analysis is used to investigate the pit growth and changes in corrosion rate with exposure time. Extreme value theory is utilized to model the maximum pit depths distribution. The probability of tube perforation due to pitting will be predicted using the Gumbel plot.

1.2 Organization

The rest of this report is organized as follows.

In Chapter 2, the theory behind the problem under study is briefly reviewed. In addition, a review on the literature on the aluminium alloys categories, pitting corrosion, corrosion of aluminium alloys, effect of chemical composition and microstructure on corrosion, statistical analysis theory, extreme value theory, and applications of extreme value theory to corrosion is presented.

Chapter 3 describes the experimental procedure used to gather the experimental data. The experimental data are used to investigate corrosion behaviour of alloys and to plot the extreme value distribution.

Chapter 4 is dedicated to the definition of statistical approach that used to investigate the pitting process in exposure duration. In this chapter, the basic theory of the Gumbel distribution and a detailed method which is used to plot Gumbel distribution and cumulative probability are explained.

The experimental and statistical results are separately presented in Chapter 5 in order to facilitate reliable discussion and conclusion.

In Chapter 6 a comprehensive discussion on the experimental results and statistical analysis is given. A parametric study is also provided.

At the end, the concluding remarks in Chapter 7 will end this report.

Chapter 2

Theory and literature review

This chapter includes two main parts; first, literature review on aluminium alloys and their corrosion properties and second, theory and background of statistical analysis .

2.1 aluminium and aluminium alloy's corrosion behaviour

2.1.1 aluminium and its properties

The properties of aluminium alloys depend on a complex interaction of alloy composition and microstructural characters created during production and thermal treatment. The application of aluminium is mostly based on three main properties; low density, the high mechanical strength achieved by suitable alloying and heat treatments, and the relatively high corrosion resistance of the pure metal [16].

2.1.2 aluminium alloys categories

A certain number of metals rather with aluminium easily but, comparatively a few number have sufficient solubility to be considered as a major alloying element [17]. Among commonly used alloying element, magnesium, zinc, copper and silicon have significant solubility, while a number of additional elements are also used because of the important improvements that they give to the alloys. Such elements are manganese, chromium, zirconium and titanium. The low yield strength of pure aluminium is the main reason of adding alloying in order to increase the strength.

aluminium alloys are usually classified with respect to the fabrication process; cast alloys and wrought (mechanically worked) alloys [18]. These two classes are further divided to categories of alloy based on chemical composition and temper designation.

2.1.2.1 Pure aluminium

The corrosion resistance of aluminium increases with increasing metal purity. In case of high corrosion resistance and ductility requirements the 99.8% and 99.9% grades are usually selected. While these products have advantages to use in chemical industry for handling, the low mechanical properties of these products limits the application to use as cladding material for stringer products.

2.1.2.2 Copper and copper–magnesium containing alloys

Alloys in which copper is the main alloying element, although other elements specially magnesium may be specified, are 2xxx series [19]. Copper is one of the most common alloying additions to aluminium because it has both good solubility and a significant strengthening effect by its promotion of age-hardening response. This series has high strength and is heat-treatable, but has low corrosion resistance, and is susceptible to intergranular attack.

2.1.2.3 Manganese-containing alloys

The manganese containing alloys up to 1% (3xxx series) are characterized by relatively good corrosion resistance and moderate strength, and the alloys can be protected in certain media[19]. Manganese has a relatively low solubility in aluminium but improves its corrosion resistance in solid solution and can moderate the harmful effect of iron-bearing primary intermetallic phases [20]. The combination of properties of this alloy in sheet form has resulted in large tonnages being used in buildings, cooking utensils, and many general engineering applications. The most common used sheet in building applications are alloys are AA3005 and AA3105, and alloys such as AA3104 are used for beverage cans because of their deep-drawing capability. It was reported [21] that 3xxx series Al alloys containing 1–1.5% manganese due to forming Al/Mn intermatellic compounds might undergo the attack of chloride ions at week defect sites. It has been acknowledged that corrosion resistance of aluminium alloy depends on formation of a layer of passive film on its surface. However, halide ions, especially chloride ions (Cl^-), show a strong attack to passive film, resulting in pitting corrosion of Al alloy.

2.1.2.4 Silicon-containing alloys

Silicon added to aluminium substantially lowers the melting point without causing the resulting alloys to become brittle which is very important and is largely the basis of aluminium casting alloys and the associated shape-casting industry [19]. The AA4xxx series alloys are both heat-treatable and non-heat treatable alloys and has good corrosion resistance and can be inhibited [18].

2.1.2.5 Magnesium-containing alloys

Magnesium that has a high solubility in aluminium impart solid solution strengthening and improvement of work-hardening characteristics. The 5xxx series alloys (containing <7%Mg) do not age-harden. When the magnesium content in the alloy is greater than 3.5%, the excess magnesium precipitates as Mg_5Al_8 . Chromium is also a common additive, and appears as a fine dispersoid of $Cr_2Mg_3Al_{18}$ [22].

Wrought and cast alloys of the AA5xx.x series have high resistance to corrosion. This accounts in part for their use in a wide variety of building products and chemical processing and food handling equipment, as well as applications involving exposure to seawater. Nominally, the corrosion resistance of these weldable alloys is good, and their mechanical properties make them ideally suited for structural use in aggressive conditions. These alloys are used both for boat and shipbuilding

An example of this series is AA5049 that are used in car industry due to its good formability (including interannealing capability) and weldability, high strength after forming, and outstanding corrosion resistance, also in the uncoated condition. In addition, AA5049 is preferentially utilized in marine environments.

2.1.2.6 Magnesium–silicon containing alloys

Silicon lower the melting point of aluminium while simultaneously increasing fluidity which make the alloy suitable for casting. aluminium alloys containing both silicon and magnesium have high resistance to corrosion specially stress corrosion cracking. These 6xxx series alloys are mainly used in extruded form, although increasing tonnages of automotive closure sheet are being produced. Magnesium and silicon additions are made in balanced amounts to form quasi-binary $Al - Mg_2Si$ alloys.

2.1.3 Corrosion and forms of corrosion

aluminium alloys may corrode through several different pathways. It is crucial to recognize the pathway or the forms of aluminium corrosion in determining the appropriate solution for each issue. When a metal is placed in an aqueous environment it can behave in three ways: corrode, show immunity or passivate [20]. The level of acidity or alkalinity of the environment significantly affects the corrosion behaviour of aluminium alloys. Passive films formed on Al alloy under various conditions are associated
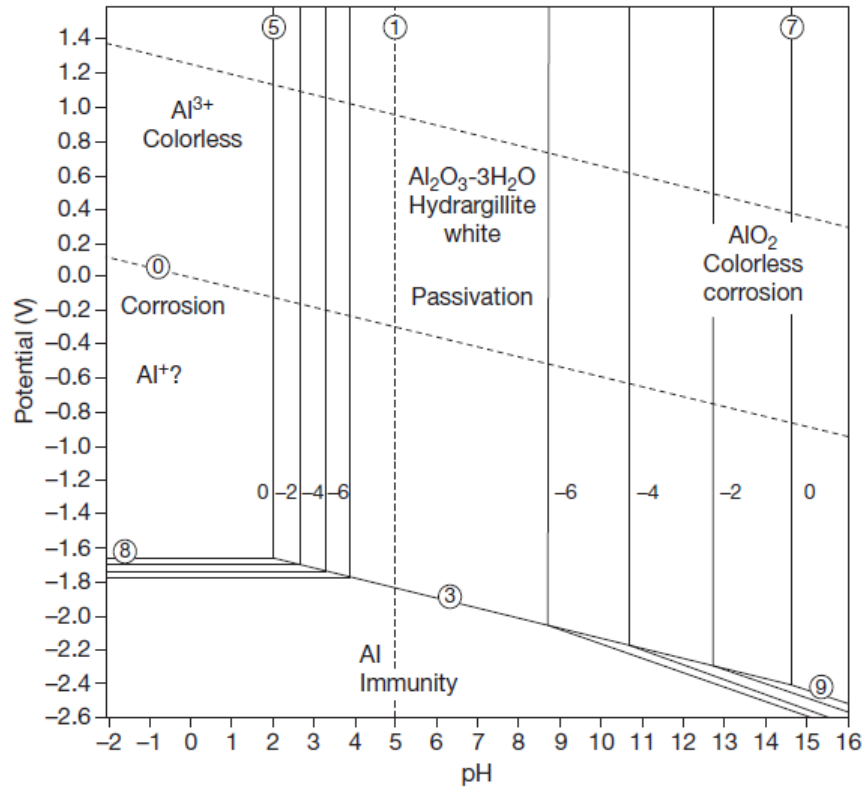
Figure 2.1: Pourbaix diagram for aluminium [23].

with different structures. For example, a thin layer of Al oxide film formed immediately in air is observed to be amorphous, while the passive film formed in aqueous solution is usually dense, coherent and compact [1]. It is expected that there are significant effects of the structure of passive film on its electrochemical and semiconducting properties, and thus the pitting corrosion resistance.

The valuable information to use in studying the corrosion phenomena is Pourbaix diagrams. Pourbaix diagrams expresses the stability conditions for protective oxide films on aluminium alloys surface (Figure 2.1). This diagram shows the thermodynamic stability of aluminium species as a function of potential and pH.

In different pH, aluminium acts in different ways. In acidic environments, aluminium dissolves as Al^{3+} ions and, in alkaline environments, aluminium dissolves as AlO^{2-} ions. The oxide film on aluminium surface is soluble in acidic and alkaline environments. Equations 2.1 and 2.2 show the anodic reactions in acidic and alkaline environments respectively and Equations 2.3 and 2.4 show the oxygen and hydrogen reduction that are the cathodic reactions in aluminium corrosion in aqueous environment.

$$Al \rightarrow Al^{3+} + 3e^- \tag{2.1}$$

$$Al_2O_2 + H_2O \rightarrow 2AlO_2^- + 2H^+ \tag{2.2}$$

$$O_2 + 2H_2O + 4e^- \rightarrow 4OH^- \tag{2.3}$$

$$2H^+ + 2e^- \rightarrow H_2 \tag{2.4}$$

It is the interaction between local cathodes and anodes and the alloy matrix that causes all forms of corrosion in aluminium alloys. These include uniform corrosion, pitting corrosion, crevice corrosion, galvanic dissolution, filforme corrosion, intermetallic particle etchout, intergranular attack, stress corrosion cracking and exfoliation corrosion. Generally, aluminium and its alloys are resistance to corrosion in mildly aggressive aqueous environments. The protective oxide layer on the alloy's surface acts as an barrier and is capable to repair itself in oxidizing environment if damaged.

In this study, the most focus is on localized corrosion specially pitting corrosion of aluminium alloys. So, a detailed overview on pitting corrosion and a small review on intergranular corrosion of aluminium alloys will be presented.

2.1.3.1 Intergranular corrosion

Intergranular corrosion (IGC) is localized attack along the grain boundaries, or immediately adjacent to grain boundaries, while the bulk of the grains remain largely unaffected. This form of corrosion is usually associated with impurity segregation effects or specific phases precipitated on the grain boundaries. In aluminium alloys, intergranular attack usually results from the establishment of local cells along grain boundaries in which second phase, intermetallic precipitates concentrate [19]; these are either anodic or cathodic to the bulk of the grain. Susceptibility to intergranular corrosion is mainly dependent upon alloy composition and heat-treatment.

The formation of intermetallic precipitates such as Al_2Cu and Al_2CuMg in the vicinity of grain boundaries makes these zones depressed in Cu content [24]. Thus, the grain boundaries become more anodic than the matrix. Hence copper-containing aluminium alloys are sensitive to intergranular corrosion .

2.1.3.2 Pitting corrosion

Pitting corrosion is a localized form of corrosion producing cavities in the material. It is difficult to detect and predict pits and also in most cases a small and narrow pit causes a failure in whole system. It can be concluded that pitting corrosion is more dangerous than uniform corrosion.

For aluminium alloys, pitting corrosion has been found to initiate at the intermetallic compounds [1]. Therefore, depending on the composition of the alloys and the environment, the pitting corrosion might initiate preferentially on different intermetallic particle types, resulting in different electrochemical behaviour [25].

The presence of an aggressive anion is a necessary condition for pitting corrosion to occur. It has been reported that such aggressive anions for aluminium and its alloys include; Cl^-, Br^-, ClO^{4-}, and NO^{3-} [26].

The pitting process can be divided into two main stages; initiation and propagation. In the initiation stage pitting starts by anions penetration into the oxide layer. The pits initiate on local sites that the passive film is damaged due to the defects or heterogeneous particles such as intermetallics. Figure 2.2 shows the propagation stage. The cathodic reactions occur outside the pit in contact with metal. Following the pH increases in the site outside the pit. The aluminium ion will form a film of aluminium chloride or aluminium oxychloride in the pit and stabilize it. Then the aluminium chloride will hydrolyze into aluminium hydroxide that causes a decrease in the pH to a more acidic environment, which increase the corrosion rate within the pit. After a while, aluminium hydroxide precipitates at the outside edge of the pit and covers the opening, that acts as a barrier to ions exchanging and reduce the rate of corrosion process.

Pits propagate in aqueous chloride ion-containing environment according to the anodic reactions

$$Al^{3+} + 3H_2O \rightarrow Al\,(OH)_3 + 3H^+ \tag{2.5}$$
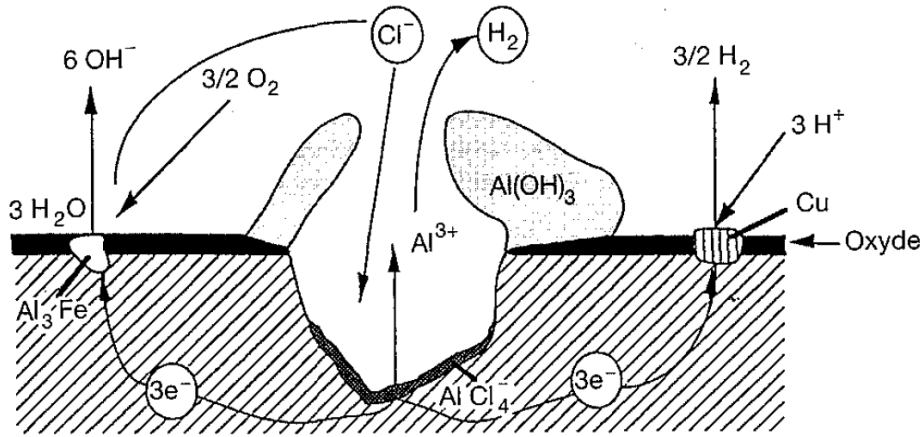
Figure 2.2: The mechanism of pitting corrosion of aluminium [21].

$$Al^{3+} + 3Cl^{-} \rightarrow AlCl_3 \tag{2.6}$$

The shape of the pit is mainly dependent on the alloy type and environment. However, the nominal shape is hemispherical [20].

The potential oscillation have been observed by many researches during pitting process [1, 27]. The occurrence of these oscillations was explained by the formation and repassivation of micro pits termed meta-stable pits.

Y. Liu et al. [6] studied the pitting corrosion of alloy 3003 in NaCl solution and found that chloride ion in passive film during the passivation causes pitting. It can be concluded that passive film that form in air is more resistance to pitting.

Kiryl et al. [10] have performed a study on the role of intermetallic phases in localized corrosion of AA5083. It was observed that iron containing intermetallics have the potential higher with respect to the aluminium matrix playing the role of effective cathodic centers for oxygen reduction causing anodic polarization and pitting in the surrounding alloy matrix. In addition, it was found that Mg_2Si intermetallics have an anodic behaviour and demonstrate partial dissolution with distinct dealloying due to selective leaching of magnesium.

Guillaumin et al. [28] showed that coarse intermetallic Al–Si–Mg-containing particles are strongly reactive in 1 M NaCl solution and seem to be nucleation sites for pits and consequently for intergranular corrosion in AA6056 alloy.

F. Lockwood et al. [22] observed that the pitting of 5052 aluminium alloy is caused by localized galvanic corrosion between aluminium metal and iron-containing constituents. Chloride ions promotes the propagation of the pits. Authors stated that different pitting process was observed on samples from different suppliers that indicates the variations in the composition of the oxide film on the alloy's surface.

2.1.3.3   Effects of microstructure on corrosion

The high amount of alloying elements added to increase the strength lead to the formation of large intermetallic precipitates during casting. Many reports have demonstrated that coarse intermetallic precipitates affect the corrosion behaviour of aluminium alloys [29, 30]. Regarding localized corrosion, the most vital character of alloy microstructures is the distribution of intermetallic particles [1]. The presence of these precipitates in the microstructure could significantly reduce alloy's resistance to localized corrosion.

The corrosion behaviour of intermetallic precipitates depends mainly upon their redox potential with respect to the matrix. Intermetallic precipitates more noble than the matrix acts as cathodes; therefore, the surrounding matrix is exposed to anodic dissolution, and localized corrosion would subsequently progress. In general, some of the intermetallic particles will show different electrochemical characteristics in the opposite direction of the behaviour of the matrix. This difference increases the susceptibility to localized form of corrosion. In this case, some intermetallic particles may be either anodic or cathodic reactive to the alloy matrix. Cathodic reactive causes alloy matrix dissolution, anodic reactive causes selective dissolution [1].

Localized corrosion is a complex phenomenon that cause a local pH gradient due to the enhanced oxygen reduction in cathodic sites and generation of hydroxyl ions. Subsequently rate and morphology of corrosion will propagate. Generally, the intermetallics which must focus on are those appear in the greatest proportion either by size or by frequency.

2.1.3.4 Corrosion behaviour of aluminium alloys

The corrosion of aluminium alloys is significantly influenced by the chemistry, and hence electrochemistry, of the intermetallic phases that populate the alloy [1, 31]. The behaviour of second-phase particles present in aluminium alloys has been studied by several authors mainly in low conductivity or chloride-containing solutions [6, 25, 26, 31]. The effect of principle alloying elements on solution potential of high-purity aluminium are shown in Figure 2.3. For each element, the significant changes that occur when the element is on solid solution state. Further addition of the same element, which forms a second phase like an intermetallic particle, causes little additional change in solution potential. Most commercial aluminium alloys contain more than one element. The effect of multiple elements (in solid solution) on solution potential are approximately additive [2]. Not only the alloying elements but also other factors such as fabrication and thermal processing and other processing factor affect the final electrode potential of the alloy.

The second phases are generally intermetallic compounds of binary, ternary, or higher-order compositions, although some elements in excess of their solid solubility are present as elemental phases. Electrode potentials of some of the simple second-phase constituents have been measured by R. Buchheit [8] and are shown in Table 2.1.

Phase	Potential, V
Si	-0.26
Al_3Fe	-0.56
Al_2Cu	-0.7
Al_6Mn	-0.76
Al_8Mg_5	-1.05
Mg_2Al_3	-1.15
Mg_2Si	-1.98

Table 2.1: Corrosion potentials for some secondary phases in aluminium alloys. Potentials are measured versus standard calomel electrode in NaCl solution [8].

Effect of copper The Cu distribution in the microstructure affects the susceptibility to localized corrosion. Pitting corrosion usually occurs in the Al matrix near Cu or Fe-containing intermetallic particles owing to galvanic interaction with the Al matrix, according to Table 2.1.

Copper-rich intermetallic particles provide sites for oxygen reduction (detrimental cathode sites), increase the alloy corrosion potential, and localize electrochemical activity on the alloy surface in a way that leads to enhanced corrosion susceptibility compared to other aluminium alloys [6]. As seen in Figure 2.3, Cu cause a shift in aluminium potential to the more positive potential. On the other hand as stated earlier, Cu acts as a detrimental cathodic site.
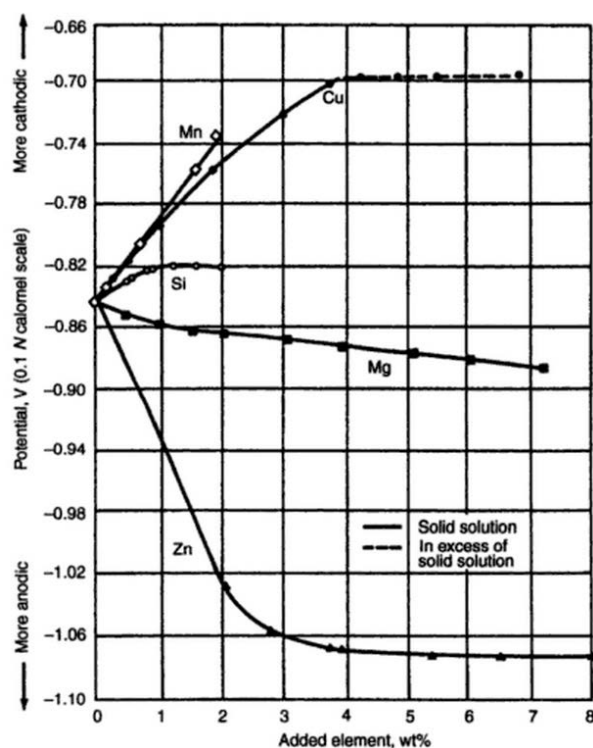
Figure 2.3: Effect of principle alloying elements on electrolytic solution potential of aluminium [2].

IGC is generally believed to be associated with Cu-containing grain boundary precipitates. Meng and Frankel [32] studied the effect of copper on corrosion behaviour of 7xxx series aluminium alloy. The authors reported that for low cu alloy small pits and semi-continuous shallow attack were found on the grain boundary while high cu alloy exhibited continuous and relatively deep IGC attack [32].

Effect of iron   Many papers were published on the influence of the Al_3Fe phase on pitting corrosion of aluminium alloys [1, 6, 33, 34]. Nisancioglu [34] studied the electrochemical behaviour of iron containing phases in aluminium alloys such as Al_{Fe}, $\alpha Al\left(Fe, Mn\right)Si$, and $\delta AlFeSi$ in NaOH solutions. Nisancioglu found that near the corrosion potential the Al_3Fe undergoes a selective dissolution of Al and the surface of the Al_3Fe crystals becomes richer in Fe. Enrichment with Fe is detrimental to cathodic behaviour.

Manganese-containing alloys   Manganese has a relatively low solubility in aluminium but improves its corrosion resistance in solid solution. The presence of Mn or Si in the phase reduces the effect of Fe on both the anodic and cathodic reaction rates. Manganese is present in the aluminium solid solution, in submicroscopic particles of precipitates and in larger particles of $Al_6\left(Mn, Fe\right)$ or $Al_{12}\left(Mn, Fe\right)_3Si$ phases, both of which have solution potentials almost similar to that of the solid solution matrix [35] that is push the solution potential to the more positive potential according to the Figure2.3. The 3xxx series, like pure aluminium, does not incur any of the more serious forms of localized corrosion, and pitting corrosion is the principal type of corrosion encountered.

The increase in the pitting potential of an $AlMn$ alloy cannot be explained by the solubility of manganese oxide which is very high. However, it can be explained by the kinetics of a pit dissolution [1]. It is known that the presence of Mn in Al increases cathodic polarization, hence decreases the corrosion rate. It is probable that depending upon the kind of alloying element a different process can determine the rate of pit growth.

Manganese containing particles such as $AlMgMn$, $AlMnCr$, and $AlMnSi$ seem to be harmless to corrosion because they ate not cathodic to the matrix [1].

Zamin [9] studied the role of Mn in the corrosion behaviour of $Al - Mn$ alloys. An increase on manganese in a solid solution causes the shift of potential of the matrix in the cathodic direction (see Figure 2.3) whereas an increase in the Mn/Fe ratio in the intermetallic shifts their potential in the anodic direction. Thus, the distribution of manganese in the intermetallics and the aluminium matrix is important. Incorporating the manganese in the intermetallics reduces the corrosion potential of the phase, as well as reducing the rate of the reduction process. Consequently, the difference between potential of the matrix and the intermetallic reduces and gives optimal corrosion resistance.

Magnesium-containing alloys   Magnesium in solid solution shifts the matrix potential to the more anodic direction according to Figure 2.3. It has been stated that Mg in solid solution does not have significant effect on the pitting corrosion of Al that it is due to the standard potentials of Al and Mg [36]. Moreover, Mg reduces the rate of the cathodic reaction (because has very low exchange current density) when present in solid solution, increasing corrosion resistance. Mg in series 2xxx, 6xxx, and 7xxx alloys forms precipitates with other alloying elements and the effect of Mg on corrosion resistance decreases [37, 38].

In regards to the 5xxx series Al-alloys, these alloys are based on additions of magnesium (Mg), along with secondary additions of manganese and often minor levels of chromium. From a corrosion perspective, β (Mg_2Al_3) phase that is formed in alloy with high Mg content at elevated temperature causes a major susceptibility to intergranular corrosion (IGC) and stress corrosion cracking (SCC).

When magnesium is present in amounts that either remain in solid solution or partially precipitate as Al_8Mg_5 particle, dispersed uniformly throughout the alloy matrix, the alloy is as resistant to corrosion as commercially pure aluminium. The corrosion potential of this particles explains this behaviour, see Table 2.1.

It is well documented that during pitting on metals such as Mg, Zn, and Al the dissolution product $MeCl_x$ forms a solid salt in pits that stabilizes the pit. Thus, $MgCl_2$ cover the opening of the pit and slows down the corrosion rate.

Magnesium–silicon-containing alloys   Al–Mg–Si (6xxx series) alloys are generally considered to have good corrosion resistance compared to Cu or Zn rich high strength Al-alloys [2]. In order to obtain an optimal combination of mechanical properties, a small amount of Cu or a large excess of Si compared to the stoichiometric Mg/Si ratio corresponding to the Mg_2Si phase is often used in 6xxx alloys [39]. This can result in an increased susceptibility to localized corrosion such as pitting and intergranular corrosion (IGC).

In a research about the corrosion of the AA6061 alloy in aerated high purity water and NaCl solutions at open circuit potential, it was found that the iron-rich particles act as cathodic sites promoting the oxygen reduction reaction, generating a localized pH increase that provokes aluminium dissolution around the particles.

In AA6061 alloy, it was found that Mg_2Si particles undergoes selective magnesium dissolution in high purity water [1]. This phase in AA5083 alloy shows anodic behaviour and undergoes partial magnesium dissolution during immersion tests in 0.5NaCl solutions . According to Table 2.1, the corrosion potential of this particle is -1.98 V that causes of selective dissolution of Mg.

In excess Si alloys, in addition to the Mg_2Si, pure Si may precipitate . These Si particles have a tendency to segregate at the grain boundaries and thereby posited to promote IGC.

2.2   Extreme Value theory

One of the main problem areas of interest to mathematicians was how to manage the values which distributed away from average values of a set of data. Some of the earliest applications of extreme value statistics were in the field of human life statistics, radioactive emission and strength of materials

[41]. The extreme value theory is becoming a powerful tool that provides the best statistical estimate of the tail behaviour of a distribution unusually large or small levels.

Within the extreme value theory, there are two primary approaches to measure the extreme values. The first is Block Maxima Models; these models consider the largest or smallest observations obtained from successive periods. This traditional approach choose a appropriate length of the periods as the blocks. Another approach called the Peak over Thershold (POT) models; these models focus on the observations which exceed a given (high) thershold. The POT models are generally considered to be the most useful applications due to their more efficient use of the data on extreme values.

2.2.1 Block Maxima Model

The concept of Block Maxima Model describes how we choose an appropriate period length, n, and block data into sequences of length. For some large values of n, this model will generate a series of block maxima, $M_{n,1}, ..., M_{n,m}$, which fit the Generalized Extreme Value distribution.

2.2.1.1 Generalized Extreme Value

Statistical extreme value theory analyses data which is experimentally gathered as the maxima of many (approximately) independent and identically distributed (i.i.d.) underlying variables [42]. The extreme value is defined, in general, as the largest value expected to occur in a certain number of observations or in a certain period of time. It can be defined on a short term basis or long term basis. In either case, however, the number of observations or a period of time have to be specified in defining the extreme value.

Using the Fisher-Tippett theorem, the family of extreme value distributions can be presented as a single parametrization form called Generalized Extreme Value (GEV) distribution. Laycock [43] illustrated the GEV as:

Suppose that $X_1, X_2, ...$ be a sequence of independently and identically distributed random variables and let $M_n = max(X_1, ..., X_n)$. Then if there exists constants $a_n > 0$ and $b_n \in R$, $(M_n - b_n)/a_n$ that is a centered and normalized maximum. If

$$Pr\left\{\frac{M_n - b_n}{a_n} \le x\right\} = F^n(a_n x + b_n) \rightarrow H(x) \tag{2.7}$$

H belongs to one of the three families of extreme value distribution functions: Gumbel (Type I), Frechet (Type II), and Weibull (Type III). The Generalized Extreme Value distribution is represented as Equation 2.8.

$$G(x) = exp\left[-\{1 + \xi(x - \mu)/\sigma\}^{\frac{-1}{\xi}}\right] \tag{2.8}$$

Where $\sigma > 0$, μ, $\xi \in IR$, and the formula is valid for $1 + \xi(x - \mu)/\sigma > 0$. The parameters μ, σ, and ξ are the location, scale and shape parameters, respectively. Evidently the value of ξ dictates the tail behaviour of G, thus we refer to ξ as the shape parameter. ξ is also called the tail index that determines the tail thickness. When $\xi > 0$, we get the Frechet distribution with $\alpha = 1/\xi$. $\xi < 0$ corresponds to the Weibull distribution with $\alpha = -1/\xi$ which is the asymptotic distribution of finite endpoint distribution. Finally, when $\xi = 0$, we have the Gumbel distribution which describes the thin-tailed distributions like normal and log-normal distributions. Frechet distribution has a lower bound whereas, Weibull has a upper bound. The Gumbel distribution is an asymptotic limit form of the largest values extracted from a parent distribution of exponential type. The unification of the original three families of extreme value distribution into a single family greatly simplifies statistical implementation.

2.2.2 Application of the extreme value analysis to corrosion

Statistical data analysis techniques have long been used in the assessment of corrosion damage to industrial plant. Such techniques are concerns about the influence of measurement error and the extrapolation of sample inspection results to uninspected areas and life prediction.

When measuring values associated with the corrosion of metals, a variety of factors affect the measured values that deviate from expected values for the present conditions. Usually the factors which contribute to the scatter of measured values act in a more or less random way. Thus the average of several values approximates the expected value better than a single measurement. A variety of distributions such as the normal, log–normal, bi-nominal, Poisson distribution, and extreme-value distribution (including the Gumbel and Weibull distribution) are observed in corrosion work [44]. If determining the probability of perforation by a pitting or cracking mechanism, the usual descriptive statistics for the normal distribution are not the most useful. Extreme value statistics should be used instead [14].

2.2.2.1 Application of the extreme value theory to pitting corrosion

For pitting corrosion, analysis of inspection data is generally focused on predicting the time at which the deepest pit is expected to penetrate through the complete thickness of the inspected item [13]. The extreme value techniques are normally appropriate for this issue. Furthermore, pits in engineering metals and alloys generally initiate at defects, such as nonmetallic inclusions or intermetallic particles, such that the number of potential pit initiation sites is typically very large. It is also well known that many pits will initiate and propagate for short periods, producing only small pits which are called meta stable pits, while a relatively small number of pits may become 'stable' and grow to significant depths.

One textbook [45] suggests that the maximum pit depth is often described by the Type I distribution, although Type III with a finite difference has been suggested. These distributions reproduce their form under maximization of further data in the same way that the Normal distribution reproduces itself under summation [13].

Generally, in pitting corrosion experiments only the maximum pit depth observed in each coupon is measured and recorded. Pit depth extreme values have shown to follow the Gumbel distribution for maxima [14, 46, 47]. Therefore, the experimental data are fitted to a Gumbel extreme value distribution, and the results are extrapolated to larger corroding areas or to longer time. By using the Gumbel fit, most of the authors have considered the pits to be independent (not interacting) identically, making the assumption that this condition is satisfied at least approximately. However, even with some dependence between pit depths (due to the interaction between growing pits), the Gumbel model can be justified to describe the pit depth extreme values [48].

2.2.2.2 Examples of applications of extreme value distribution in corrosion engineering

The applications of extreme value theory in pitting corrosion of aluminium alloys have been not published in huge number. Thus, in following paragraphs, applications of this theory for other materials will be presented as well as for aluminium alloys.

Pitting corrosion of aluminium   Aziz [14] used the method of measuring the maximum pit depth found on aluminium coupons which were exposed to tap water for various lengths of time. Aziz apparently was the first to use extreme value distribution for pitting corrosion. He used manufactured samples from different aluminium alloys. Samples were immersed in a gallon tank containing tap water. At the end of a specified time period, the samples were removed from the water and the maximum pit depth was measured and recorded. Data were plotted on the Gumbel extreme value probability paper. Graphical methods were used to estimate the parameters from the data. It was reported that there is not a significant difference in the accuracy of the graphical solution and the computer solution. As it is seen from Figure 2.4, for small pit depths there is only little variation from linearity and this part

12

obeys normal distribution. The results indicated that the Gumbel extreme value distribution can be fitted to the data.
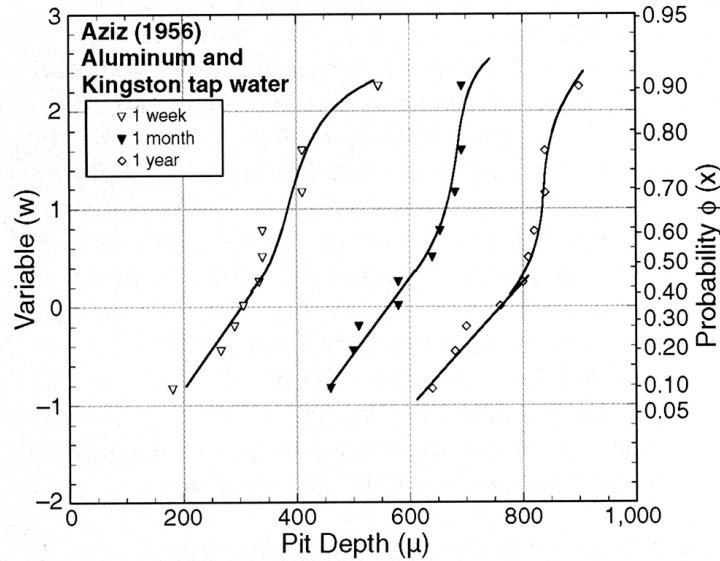
Figure 2.4: Data for maximum pit depth for aluminium in tap water and best-fit trend lines [14].

Summerson et al. [49] accurately measured thousands of pits depths that formed on different aluminium alloys samples immersed in ocean seawater at the mouth of the Halifax River for 6,12, and 24 months. The author concluded that the square root of pit depth is a better fit to the normal distribution than the actual pit depth or the logarithm of the pit depth.

Pitting corrosion of low carbon steel Rivas et al. [50] applied both the block maxima and peak over threshold approaches to extremes to pitting corrosion data from laboratory-simulated buried line pipe steel. They reported that the distribution of the maximum pit depths sampled from the BM approach is in the domain of attraction of the Gumbel subclass of the maximal GEV distribution. On the other hand, they found that the distribution of pit depths exceeding a threshold that is determined according to the POT approach is best fit by the exponential subclass of the GPD (generalized Pareto distribution). According to the extreme value statistics theory, this can be considered as a proof that the maximum pit depths were sampled from an exponential parent distribution instead of from the distribution of all measured depths. Finally they concluded that both the BM and POT methods are good approaches for analysing pitting corrosion extremes.

Rivas's work has presented an important result in the field of using extreme value theory in pitting corrosion. Their comparison between two methods BM and POT showed that POT method is less sensitive to pit dependency and give more reliable results but, it is reasonable to hypothesize that the Gumbel model can be used even with pits interaction.

Long-term marine pitting corrosion of steel It has been observed that for long-term exposures of steel to seawater the pitting process changes with exposure time and eventually becomes controlled by the rate of bacterial metabolism [11]. The change in pitting behaviour is reflected in the change in the trend of the maximum pit depth data on the Gumbel plot, particularly for longer exposures

(see Figure 2.5). Robert reported that the Frechet extreme value distribution arises naturally as the candidate distribution based on some simple modeling of the uncertainty in nutrients to the bacteria and of the proportion of pitting for a given surface. According to his study, the Frechet distribution predicts deeper pitting for given probabilities of occurrence,both compared to the conventional use of the Gumbel distribution applied to the complete extreme pit data set. This result has important and obvious practical consequences. It was also concluded that the size of coupons should be larger than those used in that work and it demonstrates the significance of experimental procedure in statistical analysis.
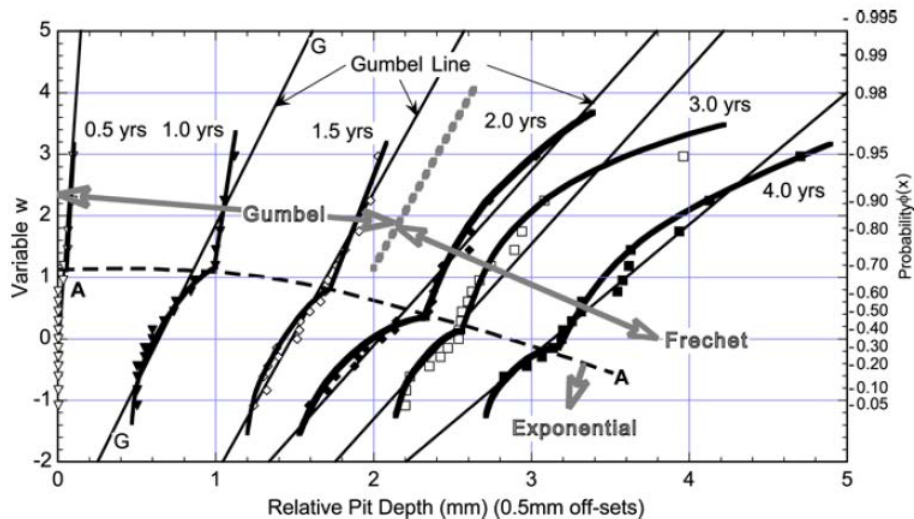
Figure 2.5: Gumbel plot for maximum pit depth for steel coupons at various exposure times [11].

Inspection of heat exchanger tubes   Heat exchanger tubes are often inspected using non-destructive testing (NDT) methods, and the results are usually reported in terms of the maximum pit depth in each tested tube. Fukuda et al. [51] introduced the use of extreme value analysis to supplement the inspection of a small number of tubes. Approximately 10-20 % of tubes are tested and the results must be used to estimate the whole tube bundle. According to ASTM G46 [52], based on the Gumbel distribution, maximum pit depths over area larger than the inspected area can be extrapolated. In Figure 2.6, the largest values of wall thinning observed for 14 tubes are plotted on the Gumbel probability paper. The distribution of wall thinning at every inspection time is seen to obey the Gumbel distribution.

14
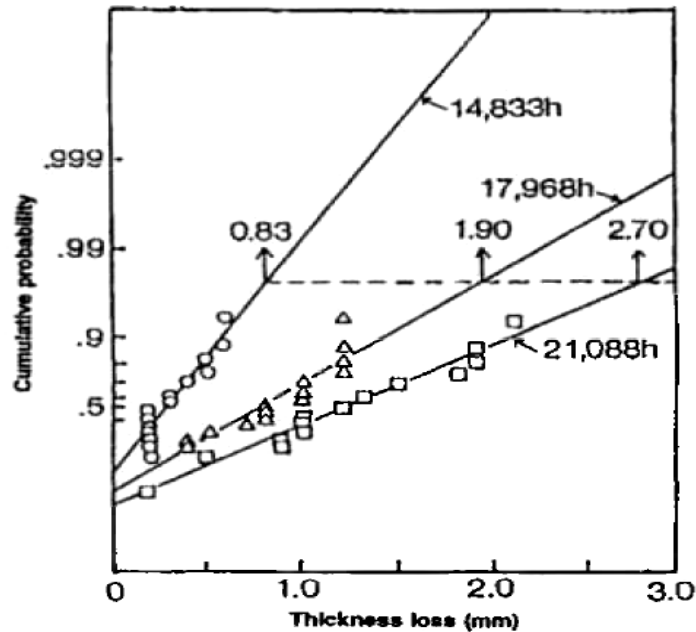
Figure 2.6: The Gumbel plots of the maximum thickness loss of boiler tubes used for different operation times [51].

Localized corrosion testing at Volvo car company   Lighter cars consume less fuel, and it is a main challenge for the automotive industry. Localized corrosion (pitting corrosion) of light metals such as aluminium or magnesium confines the use of light weight metals and alloys. A study based on block maxima and Peaks over thershold theories in Volvo Company were performed . In their approach, graphical methods were used.

Circular plates of the magnesium alloy AZ91D were combined with three different bolts and tested in climate chamber for two specific time period; 2 and 4 weeks. It was observed that in the corrosion context measuring all pits deeper than some specified thershold. It leads to using the Peaks over Thersholds method and the Generalized Pareto Distribution (GPD).

15

Chapter 3

Materials and experimental details

To investigate the overall corrosion behaviour and characterize the effect of alloying elements and mictostructure on corrosion behaviour, OCP versus time in both seawater acidified solution (SWAAT solution) and NaCl solutions, potentiodynamic polarization, and seawater acidified test were performed.

3.1 Materials

Four types of aluminium alloy were selected to study the corrosion behaviour. These alloys are from 3xxx, 5xxx, and 6xxx series and are tube shape in different diameters and wall thicknesses. Table 3.1 shows the dimension of the tubes. The microstructure of the alloys were studied using optical microscope after polishing and anodizing.

Alloy type	wall thickness μm
3003	1070
5049	1480
6061	1090
6063	1258

Table 3.1: Tubes dimension.

3.2 Electrochemical measurements

3.2.1 Corrosion potential measurements

3.2.1.1 In NaCl solution

The aim of the corrosion test was to examine how different sorts of aluminium alloys corroded in NaCl solution. The tests were performed according to ASTM-G69 standard. The samples preparation stage consisted of cutting tubes to smaller spices with length of 8 cm. The surfaces of all tubes selected for measurement, were abraded dry with No. 320 SiC grinding paper and then with No. 00 steel wool. Following mechanical preparation, the specimens were cleaned in acetone. Then, all parts of specimens except for the area that prepared for measurements $(2cm^2)$, were masked off using Beeswax. Abrading step is considered to remove the surface and record the corrosion potential of the bulk.

The test solution was consisted of $58.5 \pm 0.1g$ of $NaCl$ and $9 \pm 1mL$ of 30% hydrogen peroxide reagent per $1L$ of aqueous solution. The hydrogen peroxide was added just before measurements to avoid decomposition. The temperature of the test solution was maintained at $25 \pm 2°C$.

Corrosion potential measurements were performed as a function of time for a period of 1 h. The corrosion potential was recorded with respect to a saturated $Ag/AgCl$ reference electrode every 30 seconds for a period of 1 h. The reported potentials were converted to SCE.

3.2.1.2   In SWAAT solution

Corrosion potential measurements were performed as a function of time for a period of 24 h in ASTM D1141 synthetic seawater whose pH was adjusted to 3 with the addition of glacial acetic acid. This solution is the exact solution used in the acidified synthetic seawater (fog) test, ASTM G85-11, A3. The aim of using this solution was to obtain slow etching of the sample surface during exposure, such that the variation in corrosion potential could be recorded. In case of presence of active layer, it is gradually removed and the underlying bulk is expose to the solution. Samples were prepared according to ASTM G69 except abrading steps because the aim of the test was to record the tube's surface corrosion potential. Temperature of the exposed ambient air to the solution was approximately $25 \pm 2°C$. The solution was continuously stirred at a fixed rate by use of a mechanical stirrer. The corrosion potential was recorded with respect to a saturated $Ag/AgCl$ reference electrode every minute for a period of 24 h. The reported potentials were converted to SCE.

3.2.2   Polarization measurements

Potentiodynamic polarization was performed in stirred 5 wt% NaCl solution at $25°C$, which was exposed to ambient air. Sample preparation method was like the method used for corrosion potential measurement in SWAAT solution and the sample area exposed area to the solution was $2 \ cm^2$. Anodic polarization curves were measured with respect to a saturated $Ag/AgCl$ reference electrode in the positive potential direction, starting immediately after exposure to the solution at 50 mV below the corrosion potential. The reported potentials were converted to SCE. The cell geometry, solution volume and the stirring rate in the solution were identical for all tests.

3.3   Corrosion test

Salt spray test was performed according to ASTM G85-11, A3. Seawater acidified test, cyclic (SWAAT) started in February for all 3003, 5049, 6061, and 6063 alloys and lasted 49 days. Solution composition was in accordance with ASTM D1141. The temperature in the chamber was maintained in the range $22 - 49°C$. Specimens were cut to 20 cm length and two ends of each were blocked to prevent penetration of solution into the tubes. Specimens were cleaned in acetone before test. For each type of alloys 26 specimens were prepared and located in the chamber. Figure 3.1 shows the salt spray chamber with samples inside.
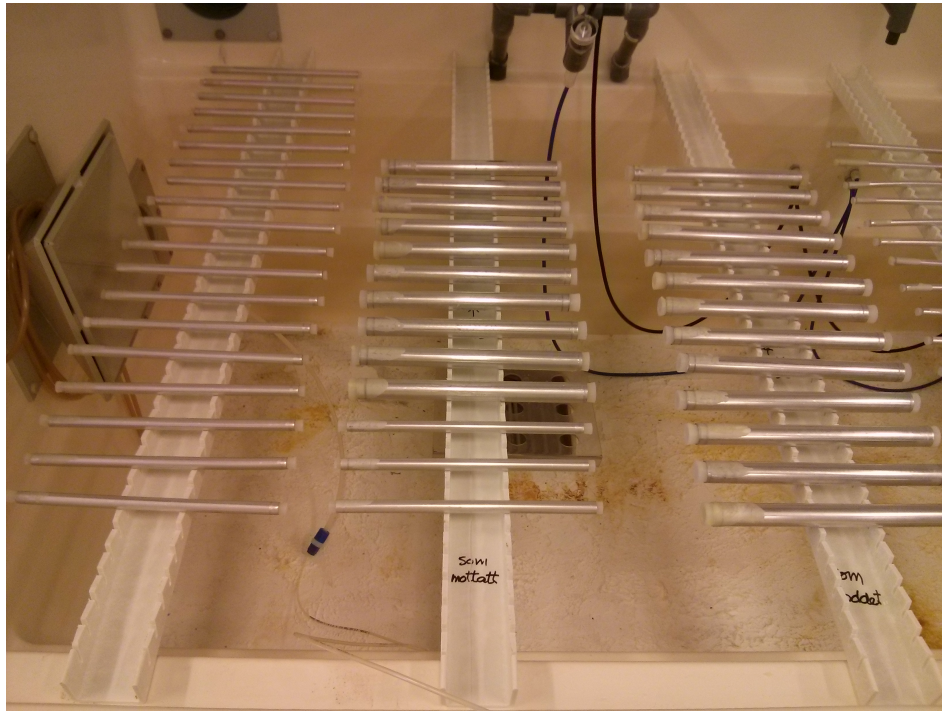
Figure 3.1: Salt spray chamber.

The samples were taken out after 2, 6, 10, 13, 17, 21, 28, 34, 38 ,45 and 49 days and washed with warm tap water. The remaining corrosion products were removed by immersion in a hot chromic-phosphoric acid solution, rinsing in distilled water and then immersion in concentrated nitric acid according to ASTM G 1 Annex A1. For alloy 3003 due to expectation of high corrosion rate different plan was chosen and samples were taken out after 1, 2, 3, 6, 7, 10, 13, 17 and 21 days.

3.3.0.1 Collection of the maximum pit depth

Samples were examined carefully for pitting and in particular for the location of the deepest pits by using optical microscope. The ten deepest pits per every sample were selected and the pit depth were measured. The deepest pits were in fact ascertained by measuring multiple pit depths and selecting the deepest. For the first 10 deepest selected pits the depth was measured using a microscope focused successively on the pit base and on the surrounding surface, thereby obtaining relative pit depth.

In addition, the deepest pits per sample were cut and the cross section were observed to measure the pit depth as an alternative method to see the uncertainty of measurements. It was found that the difference between two methods was not exceed 50 μm for 95 % of samples and for a few samples, values obtained from two methods differed around 200 μm. Then, other pits were examined again and it was decided to use the data obtained from first measurements.

3.3.0.2 Morphology

Morphology of the pit was also characterize of the cross section from the two deepest pits, by using optical microscope.

Chapter 4

Statistical analysis method

The scatter in the maximum pit depths data may be represented through an extreme value distribution. For this application the most suitable technique would be to use Extreme Value Statistics to evaluate the rate of growth of pit. Together with the log-normal distribution, it is rather common that the two-parameter Gumbel and Weibull distributions are used to describe the observed or assumed distributions of maximum pit depth and corrosion rate. It is also evident that corrosion researchers have preferred the two-parameter to the three-parameter distributions. But it should be mentioned that in most cases, simpler two-parameter distributions fit reasonably well with the corrosion data. Based on other works [44, 54, 55], it was concluded that the Gumbel distribution is appropriately fit to the maximum pit depths data. Consequently, it is assumed that data obtained in this research follow Gumbel distribution.

In following sections, the Gumbel distribution theory is described.

4.1   Gumbel distribution

The Gumbel distribution is mainly used to analyze pit depth distribution. The subset of the Generalized Extreme Value (GEV) family with $\xi = 0$ (ξ is shape parameter) is interpreted as the limit of Equation 2.8 as $\xi \to 0$, leading to the Gumbel family with distribution function given in Equation 4.1 [46].

$$G\left(x\right) = exp\left[-exp\left\{-\left(\frac{x-\mu}{\sigma}\right)\right\}\right], \ -\infty < x < \infty \tag{4.1}$$

where $G\left(x\right)$ is the cumulative probability of x (pit depth), and μ and α are the location and scale parameters, respectively. A normalized variable, y, is defined as

$$y = \left(x - \mu\right)/\alpha \tag{4.2}$$

Then $F\left(y\right)$ becomes

$$F\left(y\right) = exp\left[-exp\left(-y\right)\right] \tag{4.3}$$

$$F\left(y\right) = \frac{i}{N+1} \tag{4.4}$$

Where i is the ranking order and N is the total number of measured pit depths.

Choice to use type I (Gumbel) extreme value distribution instead of types II or III to adjust experimental data can be checked by means of formal hypothesis testing. Some of the most common tests are the likelihood ratio (LR) test and the curvature (CU) method [56].

The Gumbel plot has the vertical axis mapped in such a way that a Gumbel distribution plots as a straight line [42].

Figure 4.1 presents an example of Gumbel probability plot showing x and y scales along with F(y). One method to calculate the scale and location parameters is graphical method. According to this method, the value of x corresponding to $y = 0$ or $F(y) = 0.368$ corresponds to μ, while the slope corresponds to $1/\alpha$ in Figure 4.1.
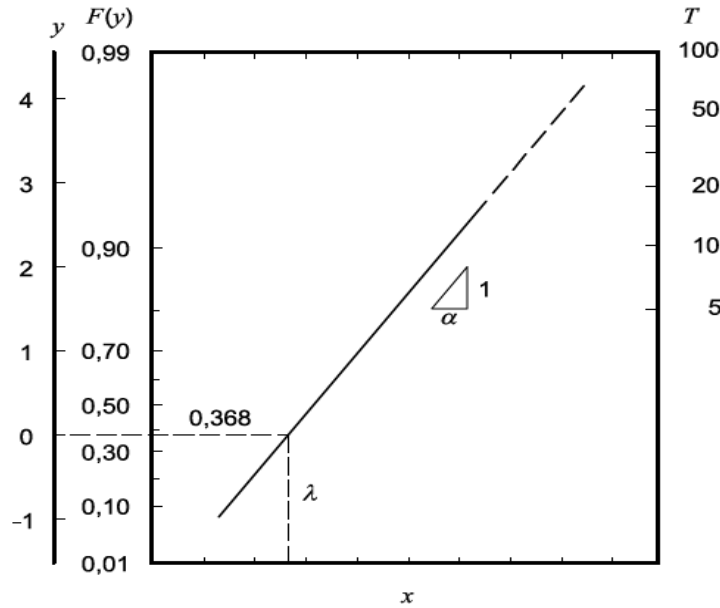
Figure 4.1: Gumbel probability paper and its coordinates [44].

An important application of the linear plots such as those in Figure 4.1 is for linear extrapolation, so as to estimate the probability of the accuracy of a given data for much larger areas, or for estimating for longer period [42].

To determine whether an extreme distribution is an appropriate model for the uncertainty associated with pit depth, it is conventional first to rank the maximum observed pit depths and then to assign each a rank order occurrence frequency. The pit depth data is, normally, plotted along the horizontal axis of so-called Gumbel Probability paper.

4.2 Method

The treatment of the data is as follows. The scatter in the data (10 pit depth per sample (x)) were arranged in order of increasing magnitude and numbered in that order. The 'plotting position' $F(y)$ of each value of x was obtained by dividing the order number by 11. The denominator 11 was used rather than 10 so that the 10th extreme could be plotted. Each value of x was then plotted against the corresponding value of $y = -ln[-ln(F(y))]$ on extreme value probability paper. The Gumbel distribution was obtained by fitting a line of y to x. If the data were indeed Gumbel distributed, each set of data points should fit well to a straight line on the Gumbel plot [42, 46]. Figure 4.2 shows the plot and the best-fit line for alloy 3003 after 7 days exposure as an example. According to Equation 4.2, the slope of the fitted line gives the value of $1/\alpha$ and the location parameter is the value of x when $y = 0$. The used method to calculate the scale and location parameters is known as graphical solution.
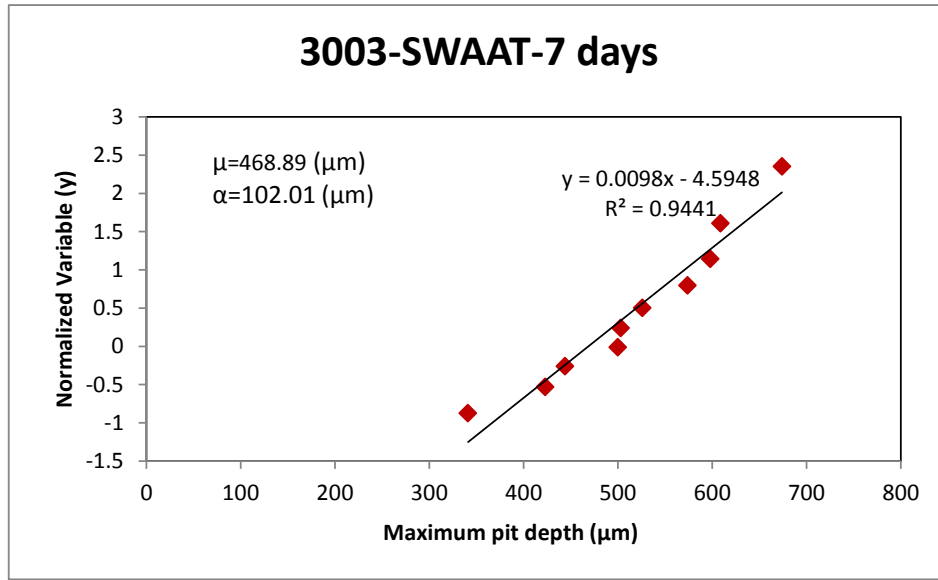
Figure 4.2: Distribution of the maximum pit depth of alloy 3003 after 7 days exposure.

Order (i)	Max. depth (x_i)	$F(y)$	$y = -ln\left[-ln\left(F(y)\right)\right]$	$F(x)$
1	200	0.0909	-0.874	0.021
2	335	0.1818	-0.533	0.210
3	375	0.2727	-0.262	0.304
4	444	0.3636	-0.011	0.473
5	500	0.4545	0.237	0.599
6	535	0.5454	0.501	0.667
7	540	0.6363	0.794	0.676
8	540	0.7272	1.141	0.676
9	593	0.8181	1.606	0.761
10	680	0.9090	2.351	0.859

Table 4.1: Maximum pit depth arranged in ascending order and calculated parameters and cumulative probability.

Table 4.1 presents the scatter data and calculations for alloy 3003 after 7 days exposure. The complete data set can be found in Appendix.

Then cumulative probability was calculated by Equation 4.1 and was plotted as a function of maximum pit depth. Figure 4.3 presents the cumulative probability plot for alloy 3003 after 7 days exposure as an example. All data were analysed and plotted in the same way as illustrated above.
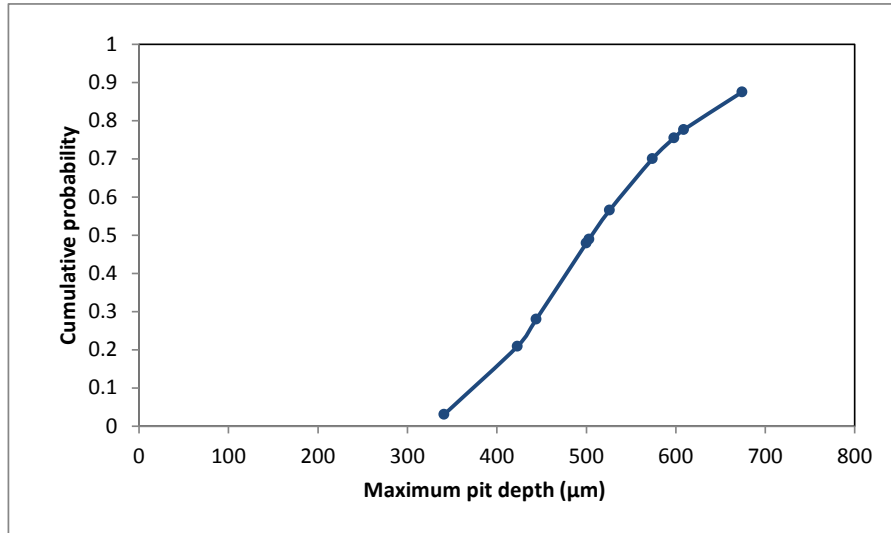
Figure 4.3: Gumbel probability plot of the alloy 3003 after 7 days exposure.

4.2.1 Extrapolation

As noted, the Gumbel distribution is commonly assumed as relevant to describe maximum pit depth data and for extrapolating the observations on small coupons to larger areas or in longer exposure time. Examination of the extreme value distribution parameters (μ and α) show that both change as a function of time, generally increasing with increased exposure time [54]. For the purpose of illustration, $x_{e(0.95)}$ that is the calculated maximum extreme value that has only a 5% probability of being exceeded, will be defined and is given by the following equation:

$$x_{e(0.95)} = \mu_e + \alpha_e.ln\left[-ln\left(0.95\right)\right] \qquad (4.5)$$

Where x, μ,and $\alpha$are in μm and t is in day.

Slopes and intercepts of the pit depth distribution plot were plotted as a function of time to find an equation to describe the changes of the scale and location parameters during the time. The functions of changing the parameters with time were found by fitting best trend to the curve.

Chapter 5

Results

5.1 Experimental results

5.1.1 Characterization

Chemical compositions of tubes are presented in Table 5.1. The major alloying elements are listed. There were also other alloying elements detected in very small amount. Figure 5.1 shows the microstructure of the samples using optical microscope. As it is seen, alloys 5049 and 6061 contain less numerous particles and more course particles than the two other alloys (3003, 6063). Alloy 5049 contain the less particles in number. In order to see the grain boundary, samples were anodized and seen by optical microscope (not presented).

(a) 3003

(b) 5049

(c) 6061

(d) 6063
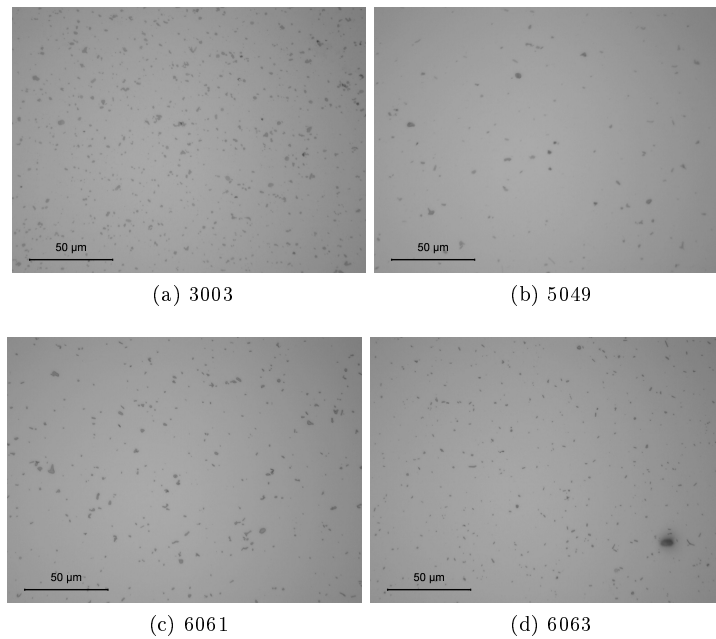
Figure 5.1: Microstructure of the alloys

Alloy Type	Si	Fe	Cu	Mn	Mg	Ni
3003	0.230	0.564	0.076	0.967	0.000	0.006
5049	0.071	0.152	0.002	0.523	1.906	0.003
6061	0.400	0.334	0.007	0.010	0.494	0.003
6063	0.432	0.197	0.011	0.035	0.455	0.003

Table 5.1: Chemical composition of alloys

5.1.2 Corrosion potential

5.1.2.1 In NaCl solution

The time dependence of the open circuit potential (OCP) is commonly interpreted as an overall indicator of the corrosion behaviour of an alloy. Figure 5.2 shows the E_{corr} variation vs. time for the four types alloy 3003, 5049, 6061, and 6063 specimens in contact with the 1 M solution respect to concentration of NaCl. In all cases except 5049, the OCP evolves toward a more negative potential until reaching asymptotically a quasi-stabilization limit. The OCP measured for the 5049 samples in a 1 M NaCl solution rapidly stabilized at a value of -757 mV$_{SCE}$ after a few seconds. It should be noted that these measurements present the OCP of bulk materials. So, the potential evolution at the beginning of the test is not important in case of this measurement.

There were fluctuation in the observed potential for all specimens up to 100 mV. For 6063, larger wavy pattern is seen and a peak up to -771 mV observed at 2730 s. Alloy 3003 showed smaller oscillation during exposure time.

The steady state OCP for all samples was taken to be the average recorded over the last 1800 seconds of measurement, given in Table 5.2. Alloy 3003 exhibited more noble corrosion potential and 6063 showed the more active corrosion potential.
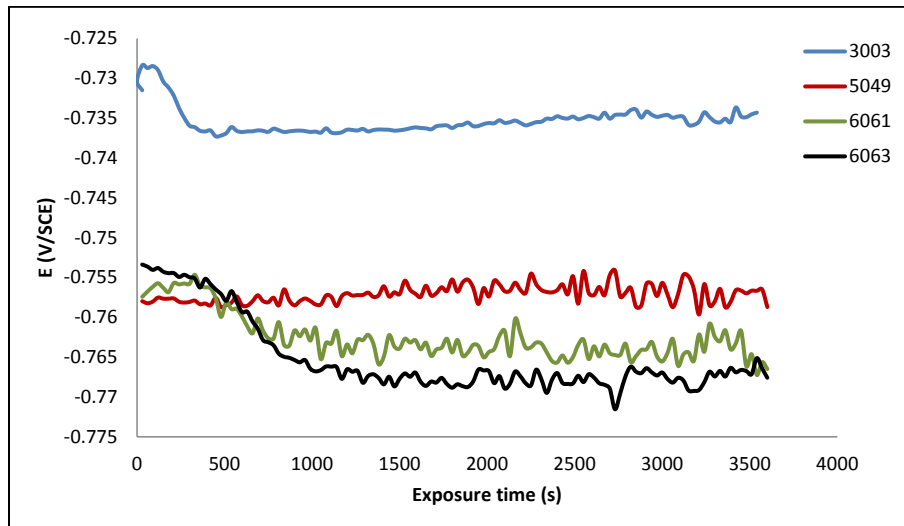
Figure 5.2: Corrosion potential variation with time measured in 1 M NaCl solution at 25°C.

5.1.2.2 In SWAAT solution

The potential-time response of four types aluminium alloy in acidified synthetic seawater is shown in Figures 5.3. As can be seen, the potential of the all alloys move in the positive direction and slowly
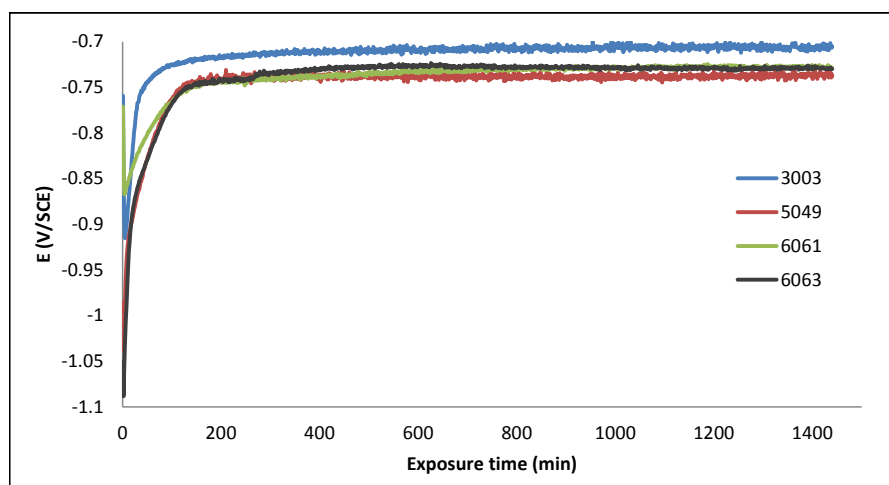
Figure 5.3: Corrosion potential variation with time measured in SWAAT solution at 25°C.

(after 2 h of immersion in solution) reaches a stable value. Shifting of the potential values of all samples to higher potential values increased with immersion time. The Oscillation of potential during exposure time is less than 5 mV.

For aluminium alloy 6063, after the initially adopted open circuit potential of -1088 mV$_{SCE}$ at the time of immersion, the potential increased at a relatively reduced rate to -745 mV$_{SCE}$ after 2 h; thereafter, the potential fluctuated in the very short range 5 mV over the following 22 h. An increase in potential up to -735 mV$_{SCE}$ is seen after 4.5 h exposure to the solution.

The potential of the 6061 alloy at the time of immersion was approximately -866 mV$_{SCE}$. The potential increases to -745 mV in the early stages of immersion in solution and remains stable all the test duration. Transient behaviour of alloy 5049 is almost the same as alloy 6063 and showed a relatively high negative potential at the immersion time. As the exposure time increases the corrosion potential of alloy 5049 goes to more negative value than 6063 and 6061. This difference is around 10 mV$_{SCE}$.

The steady state OCP for all samples was taken to be the average recorded over the last 12 hours of measurements, given in Table 5.2. It is evident from Figure 5.3 that there is no significant difference between the corrosion potential values for the 6061 and 6063 alloys. There is however a significant difference between the corrosion potentials of the 3003 and the corrosion potential of the other studied alloys. The measured OCP for alloy 5049 is is the more negative value in all studied alloys. In SWAAT solution, alloy 3003 exhibited the more positive OCP like the fact that obtained in NaCl solution.

Alloy Type	OCP in NaCl solution (mV$_{SCE}$)	OCP in SWAAT solution (mV$_{SCE}$)
3003	-735	-707
5049	-757	-738
6061	-764	-729
6063	-768	-728

Table 5.2: OCP measurements of alloys 3003, 5049, 6061 and 6063 in 1 M NaCl and AWAAT solutions.

5.1.3 Potentiodynamic polarization in 5 wt% NaCl solution

Figures 5.4-5.7 show typical potentiodynamic polarization curves for the samples of 3003, 5049, 6061, and 6063 alloys obtained in solutions of concentration 5% NaCl. The sweep measurements were started 2 minutes after exposure to the solution at 50 mV below the open circuit potential. Measurements were repeated at least three times for each alloy; the scattering for the corrosion potential values was evaluated to $\pm$ 35 mV. Corresponding electrochemical parameters are summarized in Table 5.3.

For the alloy 3003 several anodic oxidation peaks were observed specially in low current densities and low potential and a thick graph were obtained before potential equals to -737 mV$_{SCE}$. Alloy 3003 showed a relative short passive region. This result concluded from the order of passive current density of other samples.

The polarization curves of the 6061 and 5049 exhibited active-passive transitions; the alloy 5049 showed a more extensive passive region than the alloy 6061. The polarization curves clearly show a passive current density of approximately $7 \times 10^{-4}\,mA/cm^2$ for alloy 5049. The passivation region for 5049 starts at potential equals to -0.89 and the pitting will start at potential -0.73 V_{SCE}. The passive region is smaller for alloy 6061 which starts at -0.82 and ends at -0.75 V_{SCE}. Figure 5.8 shows the potentiodynamic polarization curves for all alloys in the same plot in order to compare alloys corrosion behaviour more easily.
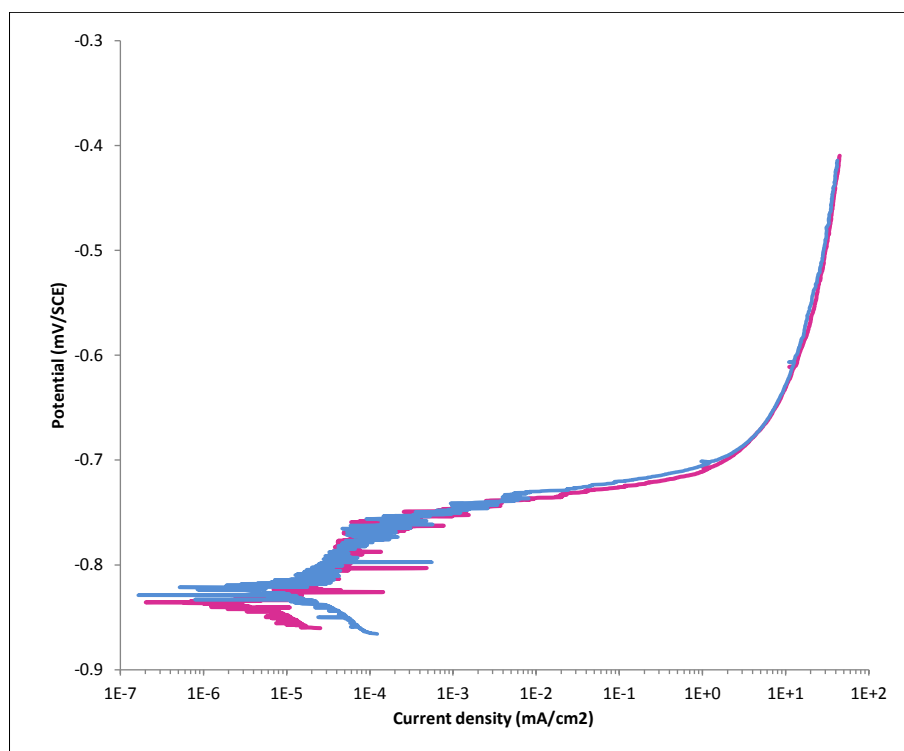
Figure 5.4: Potentiodynamic polarization curve of alloy 3003 in 5% NaCl solution at $25°C$.
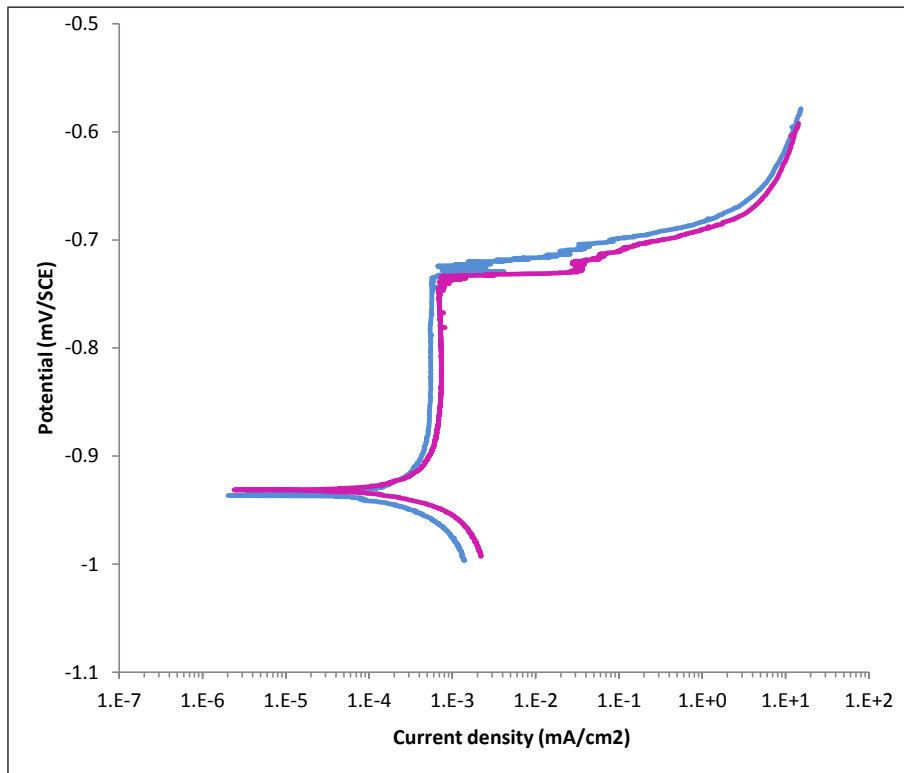
Figure 5.5: Potentiodynamic polarization curve of alloy 5049 in 5% NaCl solution at $25°C$.
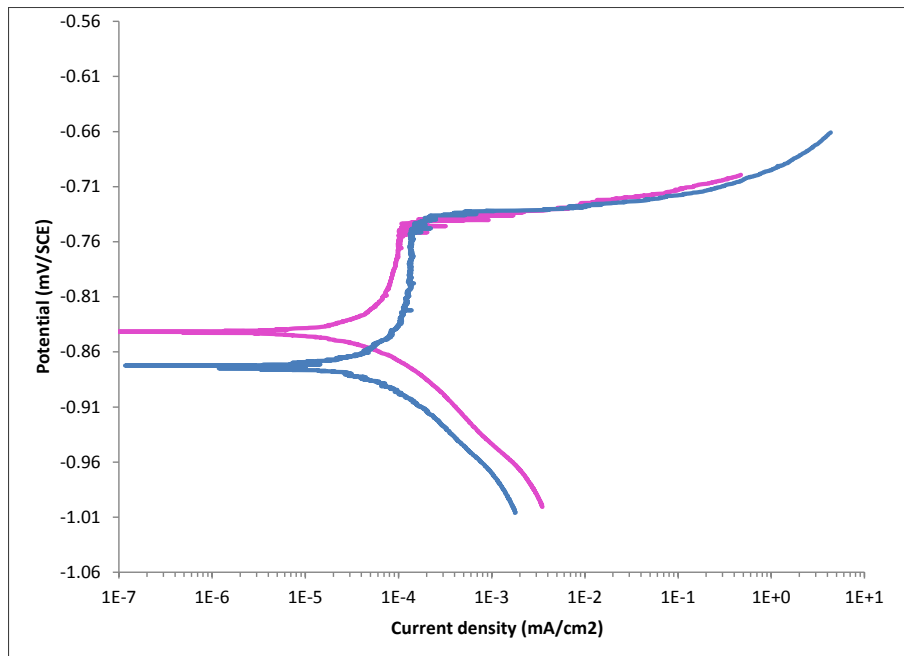
Figure 5.6: Potentiodynamic polarization curve of alloy 6061 in 5% NaCl solution at $25°C$.
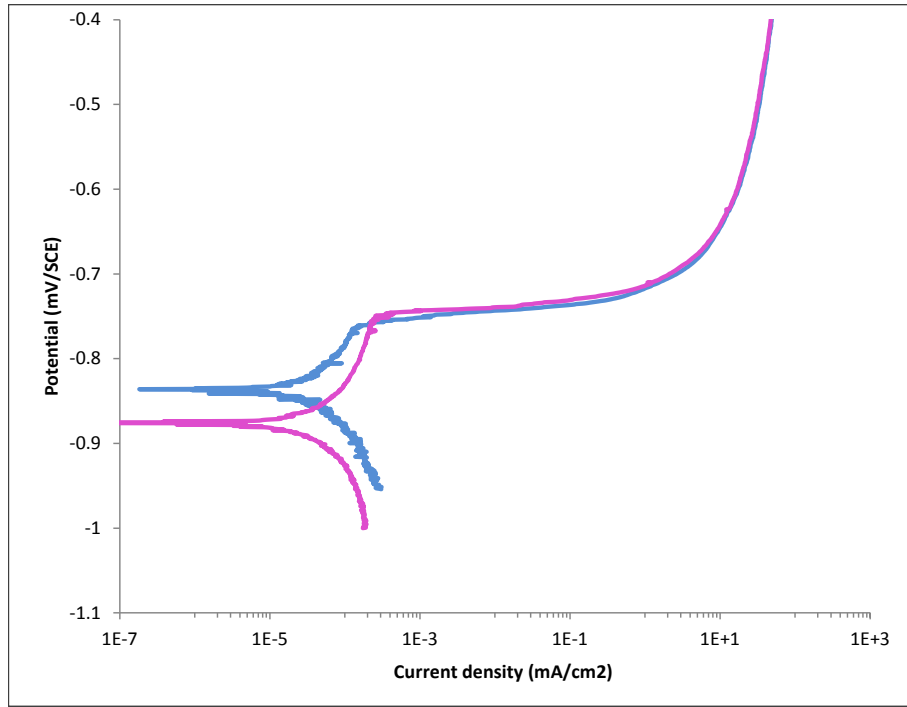
Figure 5.7: Potentiodynamic polarization curve of alloy 6063 in 5% NaCl solution at $25°C$.

Alloy's type	$i_{corr}\ (mA/cm^2)$	$E_{corr}(mV_{SCE})$	$E_{pit}\ (mV_{SCE})$	$i_{pass}\ (mA/cm^2)$
3003	3.19	-833	-766	5×10^{-5}
5049	0.87	-924	-740	7×10^{-4}
6061	0.04	-875	-736	1.34×10^{-4}
6063	3.42	-876	-752	2×10^{-4}

Table 5.3: Electrochemical parameters taken from potentiodynamic polarization curves

A similar shape is observed in two polarization curves of samples 6063 and 6061, with a little difference on their amount of noise, indeed the current density of 6061 is lower in passive region. Alloy 6063 exhibit a shorter range of passive corrosion behaviour than the alloy 6061. The onset of pitting is visible in all cases and the pitting potentials, E_{pit}, is more positive than the corrosion potentials, E_{corr}. The polarization curves for these samples showed that above the corrosion potential, the anodic current density increased rapidly showing that the samples were susceptible to localized corrosion at their corrosion potentials and an active dissolution was observed during anodic polarization. From these results, it can be concluded that the main corrosion mechanism is pitting corrosion

As it is seen from Figures 5.5 and 5.6 , there are few noises before pitting started and during the pitting progression for alloys 5049 and 6061. But, the most noisy curve was obtained for 3003. Also, these noises have been observed for alloy 6063 just before pitting started. It demonstrates the presence of meta-stable pits.

According to Figure 5.8, it can be seen that the pitting potentials of alloys 3003 and 6063 are more negative than alloys 6061 and 5049. On the other hand, corrosion potential of the alloy 5049 which has the larger passive range is more negative than the others. Alloys 6061 and 6063 showed almost the same corrosion potentials which are around -875 mV$_{SCE}$.
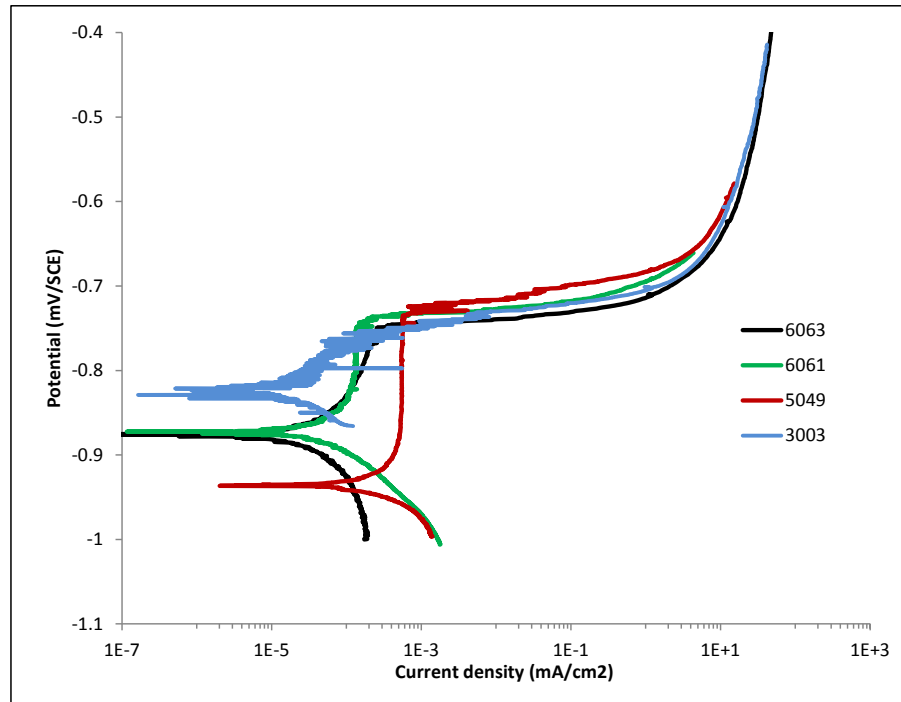
Figure 5.8: Potentiodynamic polarization curves in 5% NaCl solution at $25°C$.

5.1.4 Corrosion test

The all pit depth measurements and micro-images of some pits are presented in Appendix. Figure 5.9 shows the cross-section micro-image of a pit after 6 days exposure on alloy 3003. As seen a degree of IGC can be identified. The cross-section micro-images of pits on all studied alloys were taken and no sign of IGC was found.
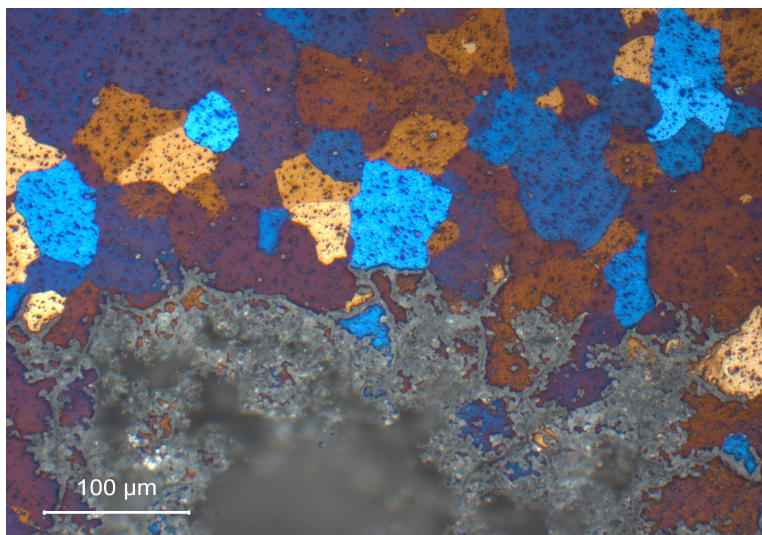
Figure 5.9: Micro-image of cross section of a pit on alloy 3003 after 6 days exposure.

5.2 Statistical results

5.2.1 Data scatter

Figure 5.10 shows the time evolution of the maximum pit depth for alloys 3003, 5049, 6061, and 6063. As it is evident, alloy 3003 exhibited a fast pitting process and reached to the maximum pit depth 1087 μm after 240 h exposure to the salt spray test. The maximum pit depth for this alloy increased with time. The rate of pitting is the lowest for alloy 5049 and the pits have not exceeded to depth more than 400 μm after 49 days exposure to the salt spray chamber. However, during the test period, there are some deviation values of maximum pit depth. Thus, it is not possible to fit a line to the time evolution of maximum pit depth. The best fits were obtained with logarithmic function for alloys 5059, 6061, and 6063. Power law gave the best fit to data of alloy 3003. Alloys 6061 and 6063 showed approximately same behaviour until day 28. After 28 days exposure, a leakage on tube of alloy 6063 was found. Considering the same thickness for alloys 6061 and 6063 will result to more pitting rate for alloy 6063. It should be mentioned that the wavy pattern of time evolution of maximum pit depth was also observed for alloys 6061 and 6063.

Figure 5.11 shows, for each alloy type, the time evolution of the average maximum pit depth distribution. The results presented in Figure 5.11 reveal that the average of the maximum pit depth distributions are distinct for each alloy series, which is especially pronounced for longer exposure time. Alloys from 6xxx series exhibited approximately same pattern while alloy 6063 experienced the leakage after 28 days. Also, It is seen that the maximum average pit depth generally increases in all cases and that there is a greater degree of scatter in the results with time according to the standard deviation. On the other hand, as it can be seen, in some data the average pit depth reduced with test duration. This behaviour has been observed for all alloys for example alloy 3003 after 10 days and alloy 5049 after 34 days. It is worth noting that the slope in the increase of the average of the maximum pit depths is lower for the alloy 5049 than other alloys. The highest rate of increasing was found for alloy 3003, specially after 10 days.

The evolution of the average maximum pit depth as a function of time cannot be fitted to the known function easily because there is a degree of fluctuation in data with time.
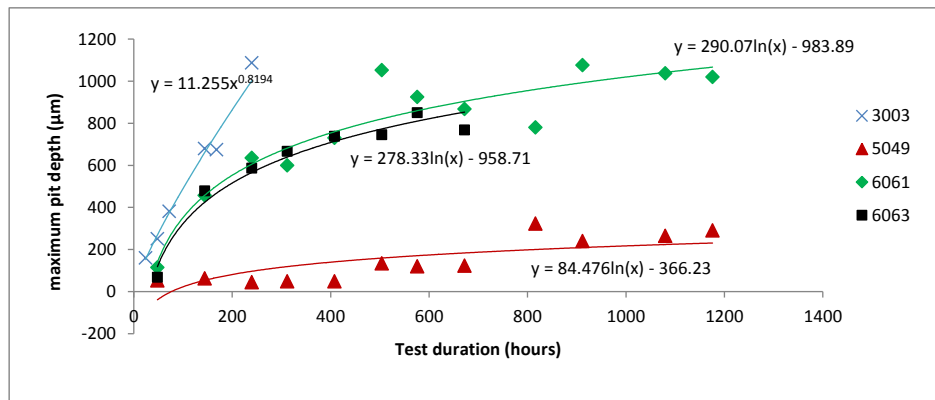
Figure 5.10: Time evolution of maximum pit depth and best fit to the data of alloys 3003, 5049, 6061, and 6063.
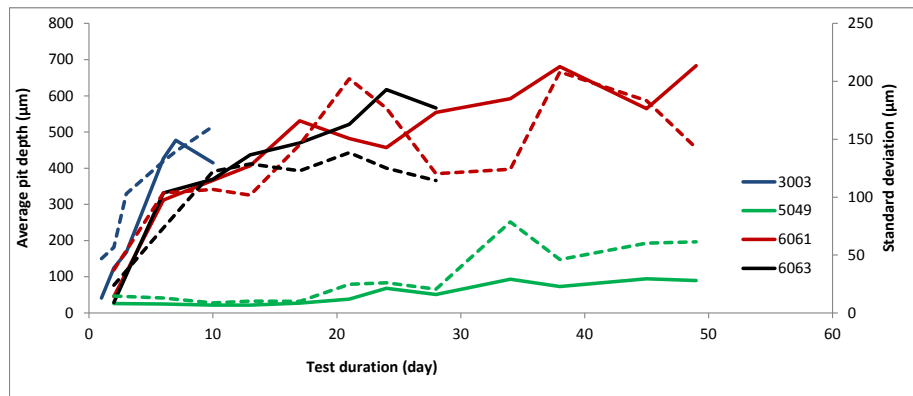
Figure 5.11: Time evolution of average pit depth of alloys 3003, 5049, 6061, and 6063. The dash lines show the standard deviation.

Figures 5.12-5.15 show, for each alloy, the measured pit depths for the 10 deepest pits at each time that samples were taken out of the chamber. In some cases it was not possible to measure 10 pits on a surface and for this reason there are, in some cases, fewer than 10 data plots recorded. For each alloy type, two samples were taken out of the chamber at the same time.

It is seen that the maximum pit depth increases and that there is a greater degree of scatter in the results with time. It is evident that at some exposure periods (after 7 and 10 days for alloy 3003 as an example) there was very considerable scatter in the pit depths recorded.
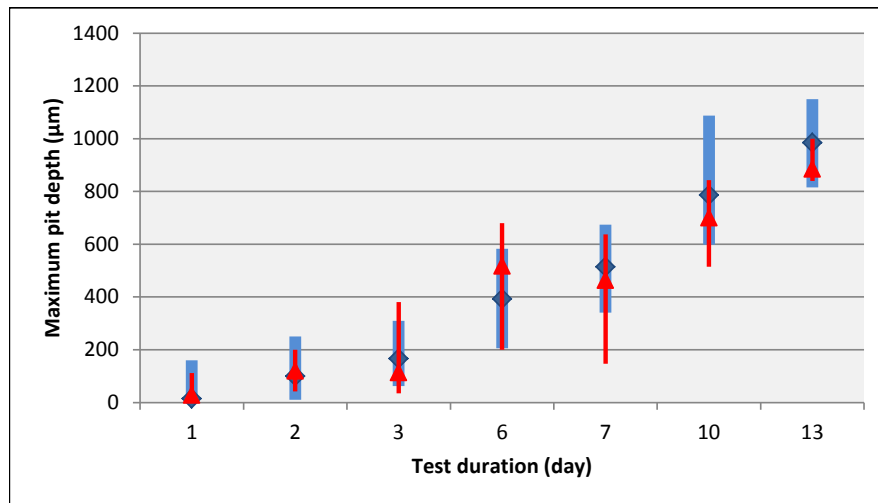
Figure 5.12: Pit depth data for observed deepest pits of the alloy 3003. 10 deepest pits were measured for two samples at the same time.
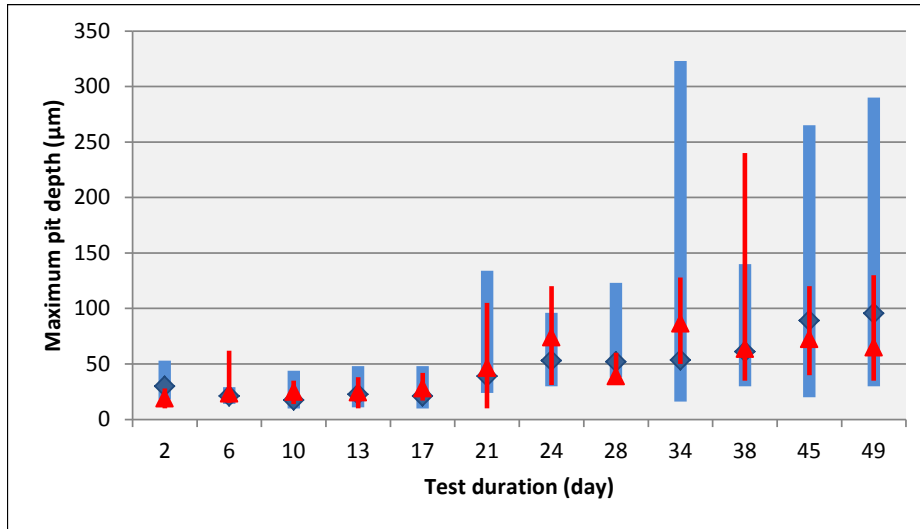
Figure 5.13: Pit depth data for observed deepest pits of the alloy 5049. 10 deepest pits were measured for two samples at the same time.
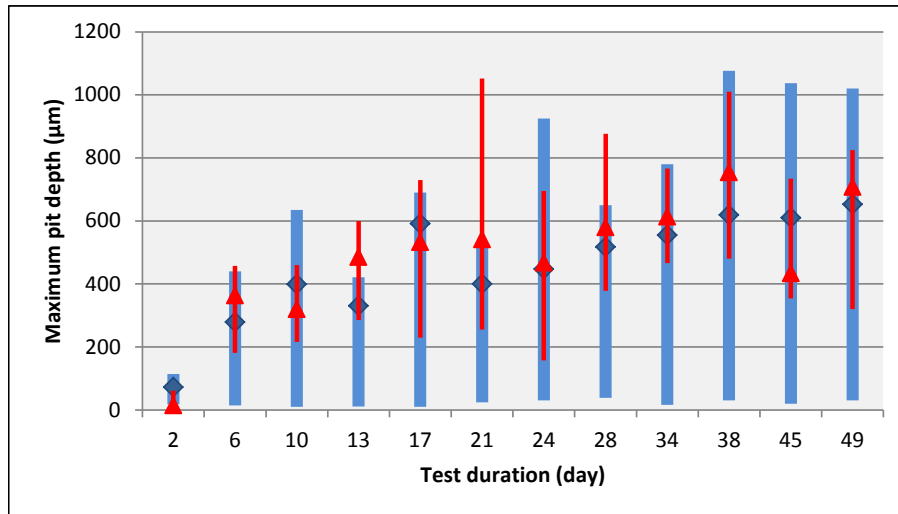
Figure 5.14: Pit depth data for observed deepest pits of the alloy 6061. 10 deepest pits were measured for two samples at the same time.
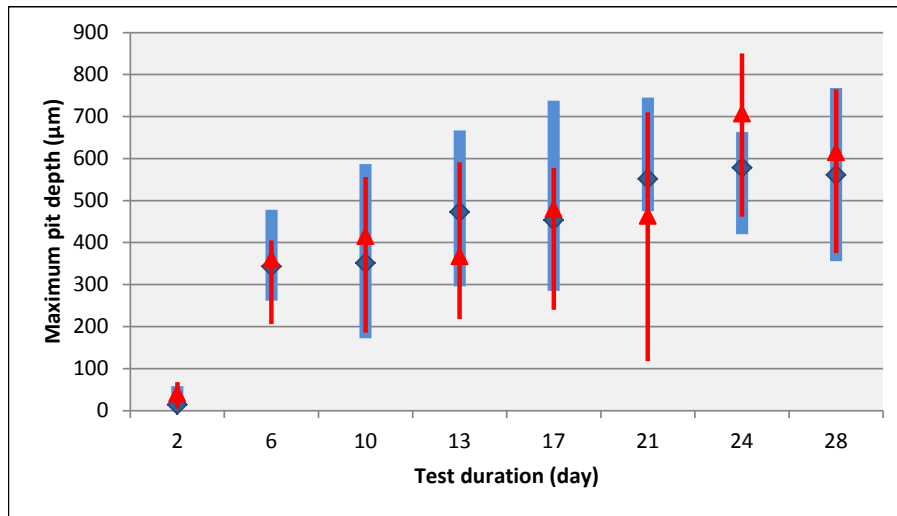
Figure 5.15: Pit depth data for observed deepest pits of the alloy 6063. 10 deepest pits were measured for two samples at the same time.

In alloy 5049, until 17 days, the dominant corrosion process is uniform corrosion and after this period pit growth takes place. Data scatter shows that although the medians of data of alloy 5049 did not changed significantly, maximum pit depths increased with time except period 38 days. Alloy 6061 showed larger scatter than the other alloys with smaller slope of line which fits to the maximum data. After 2 days exposure small pits were found and at relatively high rate pits grew after 6 days for alloys 6061 and 6063.

5.2.2 Distribution plot

The scatter in the data may be represented through an extreme value distribution, the Gumbel distribution, after first sorting the data by rank order. Results are shown in Figures 5.16-5.19 for all studied alloys. If the data were indeed Gumbel distributed, each set of data points should fit well to a straight line on the Gumbel plot. Evidently, a linear fit to the data is not absolutely perfect.

It can be seen from Figure 5.16 that as time increases graphs are shifted to the right and this behaviour has mentioned by other articles [42, 57]. Alloy 3003 exhibited leakage after 10 days exposure and data set before the leakage were used to plot distribution. As it is seen in Figure 5.16, linear fits are approximately perfect.

Alloy 5049 showed that the data for all exposure periods are approximately linear and the slopes of the linear fits decrease by increasing in exposure time, see Figure 5.17. However, for period 38 days the data trends are distinctly non-linear. In addition, by increasing in time, graph obtained for day 38 has not shifted to the right. Also, the reduced variate y vs. the measured maximum pit depth plots for longer exposure are reasonably linear according to linear regression (not shown in Figure).
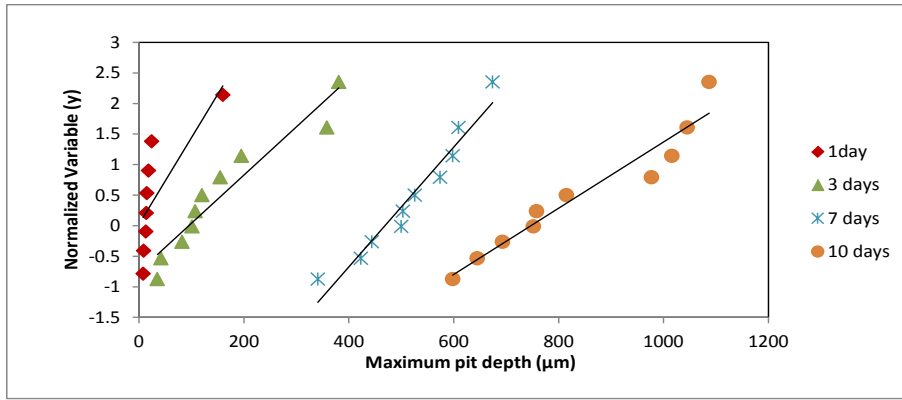
Figure 5.16: Distribution plot of the maximum pit depth for alloy 3003 with fitted lines.
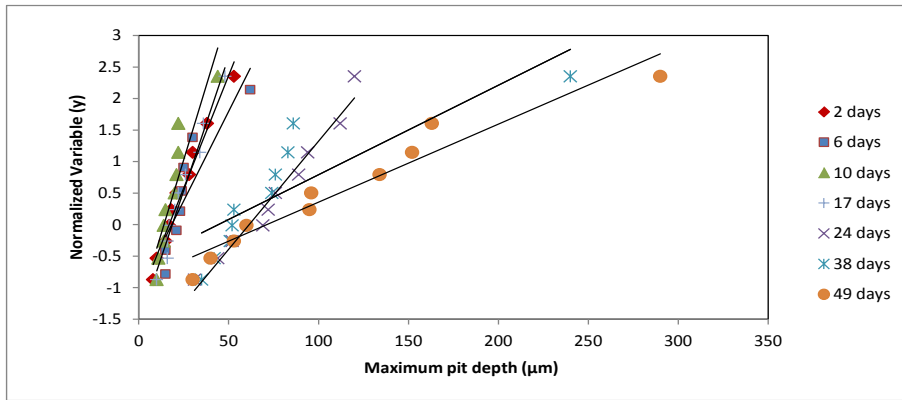
Figure 5.17: Distribution plot of the maximum pit depth for alloy 5049 with fitted lines.
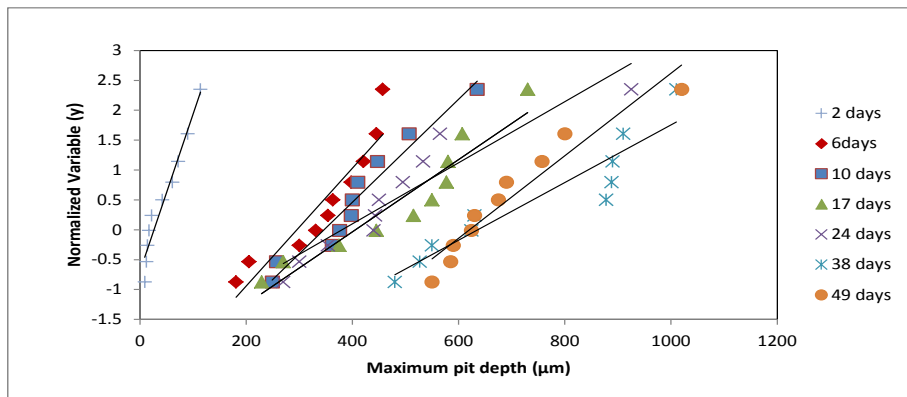
Figure 5.18: Distribution plot of the maximum pit depth for alloy 6061 with fitted lines.
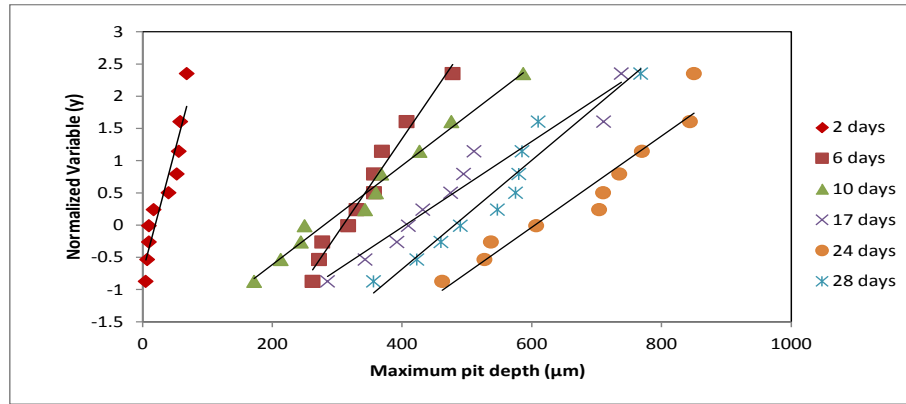
Figure 5.19: Distribution plot of the maximum pit depth for alloy 6063 with fitted lines.

It is clear that the standard fitting of a straight line through the complete data set is not a good fit for longer exposure periods shown in Figure 5.18 for alloy 6061. It is evident that the perfect linear fit were obtained until day 10 for this alloy. However, it is also clear that after 10 days period a Gumbel line can be fitted well to the lower mode data, that is, the data generated by meta-stable pitting. A closer consideration of the data relative to the best fit lines shows a degree of consistency in the variations, each data set having approximately an S-shaped trend.

Comparing results of alloys 5049 and 6061, distributions for period 38 days follow same pattern that it is unpredictable and different from other distributions at other periods. It might be due to the experimental condition.

Penetration was observed in sample of alloy 6063 after 34 days exposure in SWAAT chamber. In order to analyse more data, data from day 28 was also added to the distribution plot. According to Figure 5.19, as it is expected the slope of the fitted line decrease as time increases and perfect linear fit were obtained for alloy 6063. The same as alloys 5049 and 6061, alloy 6063 also did not exhibit a shift to the right by increasing in test duration at some periods (after 10 and 28 days).

5.2.3 Cumulative probability

The Cumulative Distribution Function (CDF) of type I extreme value model, Gumbel distribution, is given by Equation 4.1. A complete definition of equation and parameters have given in Chapter 4 by detail. Figures 5.20-5.23 show the cumulative probability of the tube being penetrated by the maximum depth pit varies with the length of exposure for alloys 3003, 5049, 6061 and 6063, based on Gumbel distribution. Standard Gumbel plot predicts greater pit depths for a given probability of occurrence.

The cumulative probability distribution plots show distinct characteristics and a degree of consistency for each alloys at different exposure duration. Thus the curves for alloys 3003, 5049, and 6063 have the characteristic of a Gumbel distribution for cumulative probability from 0 to 1, according to fitting of linear trend to the curves (not shown in Figures). This result have been also concluded from the distribution plot. The information that can be read from the cumulative probability plot differs from the one read from the distribution plot. Looking at the cumulative probability plot gives the information about occurrence probability of the maximum pit depth after specific exposure time. To illustration, it can be found that the probability of having a pit with 290 μm in depth after 49 days exposure to the sea water for alloy 5049 is 94%.
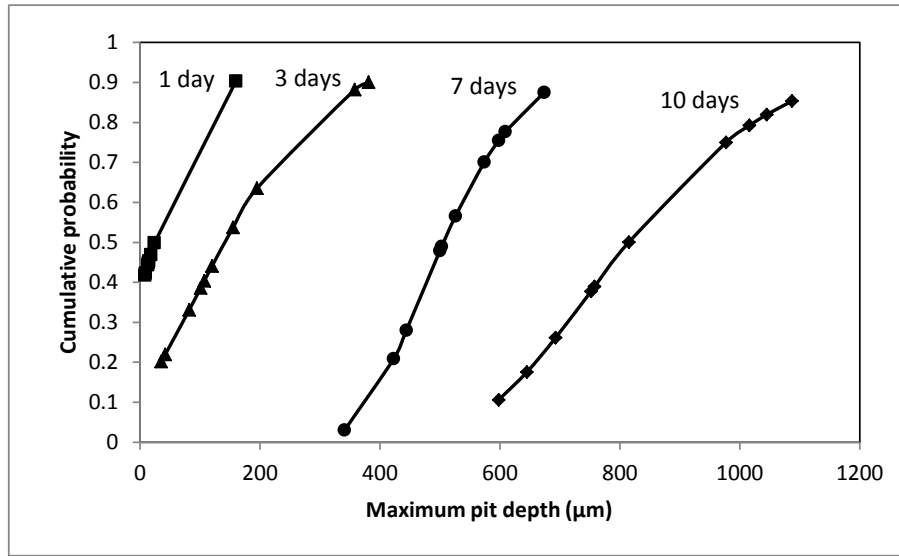
Figure 5.20: Gumbel plot for maximum pit depth from observed deepest pits for alloy 3003.
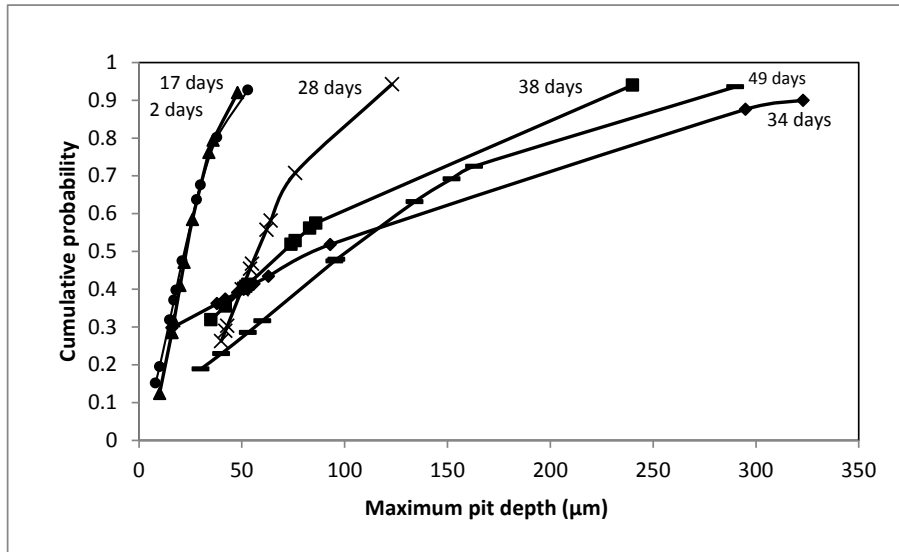
Figure 5.21: Gumbel plot for maximum pit depth from observed deepest pits for alloy 5049.
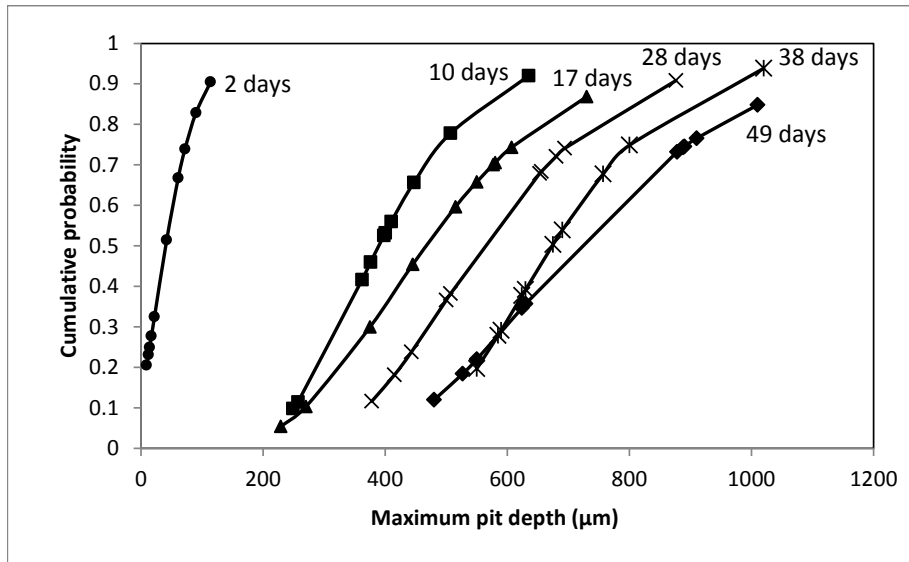
Figure 5.22: Gumbel plot for maximum pit depth from observed deepest pits for alloy 6061.
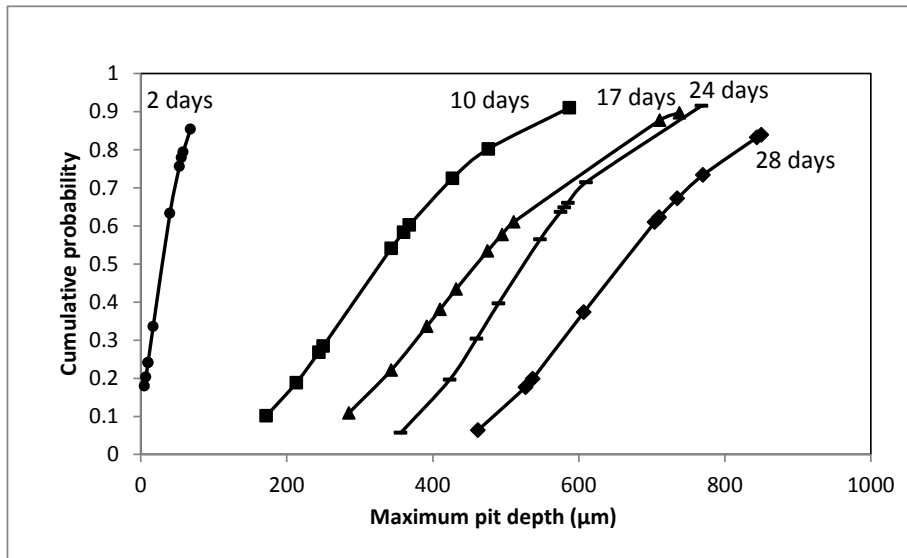
Figure 5.23: Gumbel plot for maximum pit depth from observed deepest pits for alloy 6063.

6061 shows that the probability of change-over from one distribution to the other is consistent for each data set. Figure 5.22 indicates that the data of alloy 6061 can be fitted adequately using a bi-model distribution composed of a Gumbel distribution for shallower pits and a probably Normal distribution for greater pit depths. On the other words, the higher probabilities can be plotted as Normal or Weibull distribution while for lower probability the Gumbel is perfect. Considering 49 days period, the linear fit applies for probability less than about 75% and for higher probability the linear fit does not apply.

Chapter 6

Discussion

6.1 Open circuit potential

6.1.1 In NaCl solution

The electrochemical data show clearly that alloying elements resulted in a significant change of the electrochemical properties of alloys. Evolution in open circuit potential to more cathodic direction may be corresponded to the increase in anodic/cathodic area ratio with time [58]. In addition, samples were ground before exposure to the NaCl solution. Thus the drop in potential may be the result of SiO_2 particles which remained on the surfaces of the samples.

Potential oscillation during immersion time is due to the fact that potential may arrest associated with particular phenomena. The initial growth, breakdown and partial repair of corresponding passive film may explain this general behaviour. It can also be local changes in the chemical composition of the solid solution due to dealloying. Other factors like defects, grain boundaries, voids, etc can also play role.

The high reactivity of an aluminium alloy will promote to formation of a thick protective film which indicating increasing in corrosion potential. Many researchers have discussed the open circuit potential change of the aluminium alloys in the chloride solution [59, 60, 61]. In NaCl solution, the corrosion potential shifts to cathodic value after a short period of immersion time due to the adsorption of chloride ions. The dissolution of aluminium begins from the adsorption of hydroxyl ions on the surface and aluminium hydroxide is produced by electrochemical reaction. But chloride ions also adsorb on the film and easily penetrate the hydroxide film and form a basic chloride salt [62]. It should be mentioned that the solution used in ASTM G69 is a very aggressive environment for aluminium alloys. Consequently, the oxide layer cannot remain on the surface for a long time and it forms and destroys easily causing wavy pattern.

Effect of alloying elements   Because the corrosion potential of an aluminium alloy reflects the amounts of certain alloying elements that the alloy contains, the more negative OCP values for 6061 and 6063 are due to the presence of a relatively moderate amount of Mg. Alloy 5049 also has a relatively negative corrosion potential. Generally, magnesium push the corrosion potential of aluminium to the more negative value according to the Figure 2.3. The more positive OCP of alloys 6061 and 6063 in comparison with 5049 with the highest amount of Mg may be due to the Fe content. Cathode character of iron-containing particles is the main reason of its effect. Sinyavskii et al. [12] reported that in Al-Mg-Si alloys, sensitivity to corrosion grows with increasing the content of cathode elements, in particular Fe. In comparison of two alloys 6061 and 6063 which have almost the same chemical compositions, it is noticed that the double amount of Fe in alloy 6061 has been covered by the effect of Mg. It can be concluded that even small amount of Mg can push the potential to the more negative.

A very small increase in Si content may be the other factor for more negative OCP for alloy 6063. One of the second phases in 6xxx alloys is Mg_2Si. The preferential dissolution was also found in this particle in 6xxx series [63]. It is assumed that the preferential dissolution of the matrix surrounding the coarse intermetallic particles is caused by the existence of a galvanic couple between the particles and matrix.

The presence of Cu and Fe as alloying elements in aluminium enhances the adsorption of Cl^- ions at the high negative potential leading to the dissolution of alloy.

The more positive OCP for alloy 3003 is due to the high presence of Mn. According to Figure 2.3, manganese in aluminium alloy causes a drift of potential to the more positive values. Manganese improves corrosion resistance of an aluminium alloy in solid solution. Moreover, Mn can moderate the harmful effect of iron-bearing primary intermetallic phases [20]. It has been reported that in Al-Mn alloys containing Fe, the Mn content cause a change in cathode from Al_3Fe to the $AlFeMn$ phases which have an electrode potential close to the aluminium [64]. This effect improves the corrosion behaviour of this alloys specially in atmospheric condition .

6.1.2   In SWAAT solution

All samples showed evolution to negative values when exposed to SWAAT solution. The value of initial potential is partly conditioned by that of the strength of the cathodic process, which depends on the nature of the oxidizing agent and on the cathodic area present on the alloy [59]. There are several works studied the transient in potential for aluminium alloys [58, 61, 65]. It can be deduced that the transition is due to the formation of an electrochemically active layer at the metal surface leading to the ennoblement of the electrode potential [66] or to changes in the properties of the surface oxide [67]. In other words, potential evolution to the anodic direction is often associated with the formation of a protective passive layer on the alloy surface [63]. This process is partially dependent on the type of the alloy and electrolyte chemical composition [30].

The most positive corrosion potential for alloy 3003 and more negative corrosion potential for alloy 5049 are due to the effect of Mn and Mg contents, respectively, which discussed in previous section.

6.1.3   Comparing OCPs in two environments

As seen in Table 5.2, OCPs of studied alloys in SWAAT solution is more positive than in NaCl solution in the range of 20-40 mV_{SCE} . It must be considered that measurements in NaCl solution correspond to the bulk material while OCPs measured in SWAAT solution are concerned with surfaces of the samples. It indicates that regardless of different environment the surface of sample is more resistance to corrosion than the bulk which may be due to the microstructure differences. Moreover, the difference between NaCl and SWAAT solution must be considered as well. Both of solutions are acidic. According to Pourbaix diagram, Figure 2.1, it is expected that in NaCl solution (which contains hydrogen peroxide) aluminium corrodes and in SWAAT solution passive layer forms. But, this diagram is for pure aluminium and the effect of alloying elements have not been considered.

6.2   Potentiodynamic polarization

The sweep curves of all samples were characterized by a passive region that is attributed to a passivation of cathodes on the sample surface. The relatively rough character of the polarization curves for 3003, 5049, 6061, and 6063 alloys (with low copper levels) in the passive region suggests there is much metastable pit formation below the pitting potential, since "noise" in the passive region of the polarization curves is usually interpreted physically as the formation of metastable pits that are subsequently repassivated [35].

Alloys 5049 and 6061 showed relatively low corrosion current which means less corrosion. The good corrosion resistance of these alloys probably is due to their chemical composition and microstructure. Details on the effect of alloying element are given in subsequent paragraphs.

6.2.1 Effect of alloying elements

Alloying elements such as Mg, which is more active than aluminium, oxidize first. Its oxide can improve the resistance to general corrosion when they are partially introduced into the oxide film. Alloy 5049 showed an extreme passive region that can be explained by its high Mg content and low amount of elements such as Si, Cu, and Fe. Alloying elements that are more noble than the matrix such as Si and Fe are in the form of participates or solute in matrix and form solid solution and produce a mixed-oxide film. If the participates size are in the micron range, they are not coherent with the matrix and usually remain unoxidised [68]. Alloy 6061 has a relative low Mg. Thus, it may explain the lower passivity region for alloy 6061 in comparison with alloy 5049. This difference can be attributed to the fact that the aluminium ratio in the 6061 is higher than the ratio in 5049.

aluminium may corrode because of defects in its protective oxide film. The quality of the protective oxide film depends on the purity of the alloy. Some elements like Si and Fe form second phase that are insoluble intermetallic compounds and also precipitates of compounds produced from primarily from soluble alloying elements. The low amount of Si, Cu, and Fe in alloy 5049 causes formation of a good protective oxide film on the surface of the alloy. The passive behaviour also found for alloy 6061 which contains more impurities like Si, Fe and Cu rather than 5049. In addition Mn in solid solution reduces the susceptibility to pitting corrosion and in second phase state improves the damaging effect of Cu and Fe by forming intermetallic compounds. But, Al/Mn intermetallics are active site for pit initiation. Also, the localized attacks are probably at the location of the intermetallics caused by the dissolution of the matrix around Cu and Fe-rich intermetallics. It is assumed that the local corrosion occurs at the position of layer around the $(Cu, Fe, Mn)Al_6$ intermetallic particles [60]. These intermetallics initially present an anodic character but, by selective desalting, they acquire cathodic properties with respect to the matrix. Thus, after the immersion in NaCl, localized corrosion takes place, due to the cathodic reaction that takes place over these intermetallics; this gives rise to the local increase of the pH.

Among alloys are studied in this project, 3003 and 6063 have exhibited smaller passive regions and higher corrosion current. These alloys consists of more copper (still in low amount). Copper is more noble than aluminium and in a galvanic cell aluminium will corrode in selective dissolution. According to the potentiodynamic polarization curve of alloy 3003, above E_{corr} current density increase rapidly and the corrosion rate for this alloy is too high which shows the low corrosion resistance of alloy 3003 in $NaCl$ solution due to forming a weak oxide film. On the other hand, Mn form Al/Mn intermetallic compounds which attack by Cl^-. Alloy 3003 has 1% Mn which in second phases causes pitting in alkaline environments.

6.2.2 Effect of microstructure

Microstructure also has a vital role on corrosion behaviour of aluminium alloys. 5xxx series alloys are homogeneous and corrosion susceptibility of these alloys is low due to lack of existing microstructural attack sites. On the other hand, 6xxx series alloys are heterogeneous from microstructure point of view and more susceptible to corrosion. Localized corrosion phenomena in 6xxx alloys are strongly affected by the chemistry, dimension and distribution of the intermetallic particles and precipitates [39]. The presence of coarse participates in aluminium alloy microstructure significantly diminish the material's resistance to localized corrosion. The nominal precipitate that can form in 6xxx series in the range of compositions studied is Mg_2Si which is an anodic participate [7]. Also, the presence of Cu-rich film along the grain boundary along with presence of coarse particles in 6xxx alloys with small amount of Cu have been found by G. Svenningsen et al. [69]. It demonstrates the microgalvanic coupling between these cathodic sites and matrix causing IGC. Godard et al. have found that Al–Mg–Si alloys generally corrodes significantly faster than Al–Mg alloys [70].

The effect of microstructure on lower corrosion resistance of alloys 3003 and 6063 can be demonstrated by the fact that the presence of a higher density of intermetallic particles has significant effect on the cathodic reaction: The greater the number of intermetallic particles, the greater the cathodic reactivity. As see in Figure 5.1, alloys 3003 and 6063 consist of more numerous particles in their

microstructure. On the other hand, the character of the intermetallics has a significant effect on their reactivity and it is not possible to discuss the effect of amount of particles without having their chemistry.

6.2.3 Comparing results from OCPs measurements and potentiodynamic polarization

To compare the corrosion potentials with the OCPs measured in potential transient tests, two points must be considered. First at all, OCPs measured according to ASTM G69 are related to the bulk material. Secondly, different solutions influence the corrosion process differently. According to data from Table 5.2, corrosion potential of all alloys are much more negative than the OCPs measured in SWAAT and NaCl solutions. In ASTM G69 test, exactly before running the test, hydrogen peroxide was added to the solution. So, both SWAAT and G69 solution are so aggressive. It can be concluded that the OCPs measured can correlated to the pitting potential according to the result from potentiodynamic measurements.

In conclusion, OCPs measurements are not sufficient data to study the corrosion behaviour of aluminium alloys. An additional test, like potentiodynamic polarization is require to see how an Al alloy behave in any environment.

6.3 Statistical discussion

6.3.1 Pit depths evolution

The time evolution of maximum pit depth and also average maximum pit depth gives information regarding pit growth during exposure period. Usually the factors which contribute to the scatter of measured values act in a more or less random way so that the average of several values approximates the expected value better than a single measurement. However, in studying pitting corrosion the maximum pit depth is more important than the average pit depth because perforation is caused by the deepest pit. As seen from Figures and , evolution of maximum pit depth and the average value show same patterns. Otherwise, evolution of average maximum pit depth could be useful to attain information regarding pitting corrosion rate.

The nonconsistancy in increasing the maximum pit depth with time for alloys 5049, 6061, and 6063 show that there is a substantial increase in pitting corrosion behaviour after a period of gradually declining instantaneous corrosion rate. This can be probably due to the; (i) corrosion process changing, (ii) variability in pit depth due to the influence of microstructure of the alloys, (iii) measurement's error, and (iiii) pits stochastic nature. To explain the first reason, there is probably changes in the corrosion process, starting with very rapid pit initiation, followed by an oxygen diffusion rate controlled oxidation process (concentration control, diffusion control) and eventually, at a period of exposure, a relatively sudden increase in the rate of corrosion takes place. Following this the corrosion rate then tends to decrease with further exposure. Stable pits develop under diffusion control and the extreme pit depths are the depths of stable pits. In pitting corrosion theory, this is explained by the fact that, for sufficiently long exposure, the deepest pits are the most likely to grow. Consequently, the range of pitting rates is primarily determined by the growth rate of the deepest pits. These pits grow with a steadily decreasing rate because of the stability attained during the long term, diffusion-controlled pit propagation [71, 72]. Seemingly, the stability of pit growth and other factors, such as the build-up of corrosion products, also reduce and stabilize the variability of the pitting corrosion rate as the exposure time increases.

As seen in Figure 5.11, the standard deviation of average maximum pit depth has not saturated even after long exposure. This should correspond to the fact that pit growth has not reached the equilibrium in all alloys.

6.3.1.1 Effect of alloying elements and microstructure

It is evident from Figure 5.11 that alloy 5049 is more resistance to pitting corrosion and alloy 3003 showed the highest corrosion rate. The differences have been attributed to differences in microstructure and chemical composition. The lowest corrosion rate of alloy 5049 can be explain through its chemical composition and microstructure. As seen in Figure 5.1, the number of inclusion was less numerous for alloy 5049. Such localized microstructures are well-known as potential sites for pit initiation [62]. Moreover, as stated earlier alloy 5049 showed a wide passive region due to its high Mg content. These explain the high corrosion resistance of alloy 5049 from microstructure and chemical composition view points, respectively. There is also some empirical support that small differences in composition can influence the depth of pitting [54]. The content of copper in alloy 3003 caused some degree of IGC that is one of the reasons of higher corrosion rate of this alloy, see Figure 5.9. Also, this alloy has a relatively high amount of iron that expresses the view that iron-rich inclusions act as cathodic sites for oxygen reduction and generate a high local pH that initiates pitting corrosion.

The same behaviour of alloys 6061 and 6063 in evolution of maximum and average pit depth is due to the almost same chemical composition. On the other hand, the small difference in amount of Mg, Fe, and Si caused a higher corrosion rate after 28 days for alloy 6063. The larger passive region for alloys 6061 and 6063 compare to alloy 3003 is the main reason for lower corrosion rate of these alloys. It can be concluded that even in so aggressive environment, the passive film can reduce the pitting rate. The effect of alloying elements on corrosion resistance and passivity of alloys have been discussed by detail in Sections 6.1.1 and 6.2. It is worth to conclude that the data from potentiodynamic polarization measurements are in agreement with SWAAT test.

6.3.1.2 Application of electrochemical measurements in corrosion investigation

potentiodynamic polarization curves showed that the OCPs obtained in potential transient tests are more positive than corrosion potential found in sweep measurements. It indicates that OCPs can correlated to the pitting potential according to the potentiodynamic polarization curves. However, a good agreement between potentiodynamic polarization and result obtained from SWAAT test was found. Consequently, it is suggested that OCPs measurements are not useful to determine the corrosion resistance of aluminium alloys, at least for alloys studied in this project.

6.3.2 Data Scatter

Studying how maximum pit depths scatter for every single sample also gives information about corrosion rate and the type of pits. In Figures 5.12-5.15 it is evident that at some exposure periods (longer exposure) there was very considerable scatter in the pit depths recorded. This is consistent with findings earlier for coupons of mild steel [42, 55], and is the result of variability in (i) the change in the governing corrosion process and (ii) the possible influence of microstructure in the corrosion process for longer exposures [73].

In 3003 alloy, until 3 days, line which medians are forming has a little slope which indicates during this time corrosion is partially uniform and small pits were initiated. After longer period, pitting takes place in higher rate which is due to the corrosion process changing and stochastic nature of pits. The higher rate in increasing of maximum pit depth comparing with the median shows that the deepest pits effectively grow faster than the rest of pit population.

The wide distribution range for alloy 6061 indicates that its distribution follows the underlying distribution which will be discussed further. The way that maximum pit depth scatter significantly affects the type of distribution which can use to predict life time.

6.3.3 Pit depths distribution

Linear fit to the distribution plot demonstrates the Gumbel distribution. A huge number of researches have proved that most maximum pit depths data are distributed as Gumbel distribution. It was found

that the linear fits are not absolutely perfect for alloys 3003, 5049, and 6063 but, the fitted lines are reasonably linear according to linear regression. Typically, any variability of the data regarding the best fit lines is attributed to a sampling error and to natural variability [42]. Good straight lines, the slope of which, however, changes with time, indicate that the extreme value distribution, type I, can be fitted for the whole data for alloys 3003, 5049, and 6063.

Note that the straight lines shift to the right and rotate clockwise with increasing exposure time, indicating that the location, as well as the scale parameters, increase with time. This kind of variation of the position and slope of the Gumbel straight lines has been associated with well-controlled pitting corrosion experiments [14, 74]. This behaviour is connected with the increase of average maximum pit depth and the broadening of the maximum pit depth distributions with increasing exposure times. The general indication of these changes is that the corrosion rate increases with time which is related to the decrease in the slope of the trend. As seen from Figures 5.16-5.19, corrosion rate increases with time that is due to the higher corrosion rate for stable pits after longer exposure time. Comparing all alloys shows that alloy 3003 exhibited the higher corrosion rate and alloy 5049 showed lowest corrosion rate. Alloys 6061 and 6063 showed approximately the same rate until day 28 and after that alloy 6063 exhibited higher rate. The difference between alloys can be attributed to their different chemical composition and microstructure which discussed earlier. It is important to state that same result were observed in potentiodynamic polarization measurements.

Why different distribution for alloy 6061? Examination of the pitting data in extreme value analysis showed that homogeneity of the data is one of the necessary and required assumption. Modern understanding of pitting behaviour suggests that this is not a valid assumption. Also, in current project and in most previous research applications of the Gumbel distribution there has not been sufficient maximum pit depth data at any one exposure period for constructing a Gumbel line. Moreover, it has been reported that extreme value experience will always have an intrinsic scatter, even if a good sampling procedure is used. Consequently, it is expected to obtain result which cannot be fitted to the straight line.

Approximately, S-shape trend to the data of alloy 6061 after period 10 days indicates that there may be an alternative fit to the data. Laboratory observations of a huge number of statistical studies on pitting corrosion show that the statistical distribution of pit depths change with time. The initial pit depths appear to be exponential and distributions suggested for the depth developed pits include log-normal, normal, and extreme value [57]. Scientists suggested that for deeper pits Normal distribution may be the best choice.

It is vital to stress the phenomenon of stable and meta-stable pits. While the distinction between stable and metastable pitting behaviour is well-known in the pitting corrosion literature, it does not appear to have been exploited for the statistical analysis of extreme pit depths. Its importance lies in the fact that this phenomenon causes an existence of (at least) two different statistical populations; (i) pits belonging to the regime of immediate initiation and mainly stable pitting, and (ii) pits belonging to the regime of delayed initiation or meta-stable pitting [42].

A new category of pits, the so-called 'super-stable' pits was defined to denote the category of stable pits that are initiated immediately at first exposure and then grow in depth at the fastest possible rate consistent with material and environmental constraints [75]. It follows from the fact that meta-stable pits have a different behaviour pattern from stable pits and therefore form a different population. Moreover, except under very short exposures, the meta-stable pits can never be deeper than the stable pits and the super-stable pits can be considered as the extremes of the stable pit population.

It is clear that the standard fitting of a straight line through the complete data set is not a good fit for any of the exposure periods for alloy 6061. However, it is also clear that a Gumbel line can be fitted well to the lower mode data, that is, the data generated by meta-stable pitting. On the other hand, extreme values, attributed to the super-stable pits and stable pits, did not follow the Gumbel distribution. Two distributions can be suggested according to the results and literature; (i) bi-model distribution consists of Gumbel for lower mode data and Normal distribution for upper mode data, (ii) Weibull distribution. It is important to stress that current discussion is mainly based on literature

and the only suggestion that has been examined was Gumbel distribution.

The distribution plot of alloy 6061 displayed some degree of affinity with the underlying pit depth. Reference to the corrosion literature shows that such a bi-modal distribution is commonly observed for the underlying pit depth distribution, that is the probability distribution for all pits of measurable depth [14]. As seen in Figure 5.14, wide scatter of data have measured for alloy 6061 that indicates the fact that meta-stable pits are included as a large section of data at any exposure. There are three possible issues that arise [73]: (i) sampling representativeness, (ii) homogeneity of the pit depth sample data and (iii) whether the extremes are independent events as required by extreme value theory. It can be suggested that by choosing only 5 deepest pit per sample, the fitted lines would be linear and complete data may follow the Gumbel distribution.

6.3.4 Cumulative probability

In particular, the answers to many basic questions may be read directly from the Gumbel plots. When a Type 1 Extreme Value distribution has been identified, estimation of corrosion rate can be carried out using the probability plot, Figures 5.20-5.23. In this case it can be seen that the graph shifts across the pit depth axis in time. The rate of corrosion can be estimated from the shift. As seen in cumulative probability curves, curves of alloy 3003 showed larger shift to the right with time that indicates higher corrosion rate. On the other hand, for alloy 5049 as time increases the probability curves shift to the right at very small scale. These results are in agreement with electrochemical results. Potentiodynamic polarization curves showed large passive region for alloy 5049 in comparison with other alloys. The agreement between results from potentiodynamics measurements and Gumbel plots states that the extreme value statistical analysis can be used to study the corrosion of aluminium alloys to predict the life time of a structure.

For alloy 6061 with bi-model distribution, the cumulative probability also can be calculated using two different analysis method; for higher cumulative probabilities, Normal distribution and for lower cumulative probabilities, the curves fit to the Gumbel distribution. This indicates that the Normal distribution that may be fitted to this data gradually becomes dominant with longer exposures. In some literature of application of extreme value to the pitting corrosion, different distributions were applied to bi-model data. Melchers [42] have studied the statistical analysis of pitting corrosion of mild steel in sea water. The bi-model was found like the behaviour found for alloy 6061 in this project. The author compare the Gumbel plot with the two different plots including a Gumbel for shallow pit and Normal plot for deep pits. It has been concluded that fitting Gumbel distribution to the complete data can be considered as the good fit. In addition, using a mix population of pits is well-known to increase the level of uncertainty.

In current study, the deviation from linearity is so great for alloy 6061 after 10 days exposure that the Gumbel distribution is clearly not the best fit for whole data set. Moreover, according to the literature, the probability distribution for the extremes data of alloy 6061 might be similar to the underlying probability distribution for all pit depths. It is likely that this is the result of a high degree of dependence between pit depths. For pitting, it is very unlikely that the pit depths are statistically independent [76].

6.3.5 Extrapolation

Since the Normal distribution is much less heavy-tailed than the Gumbel distribution it provides much less conservative estimates for the occurrence of pits deeper than observed [77]. It was found that distribution of data gathered for alloy 6061 follows bi-model distribution. Thus, the extrapolation were calculated only for alloys followed Gumbel distribution.

Fig. 2 shows the relative pit depth data (i.e., without correction for general corrosion) plotted on Gumbel paper and the best fit straight lines consistent with the data. These lines can be extrapolated beyond the range of the data as shown. It is then possible to estimate the probability of occurrence of a particular depth of pit in a given exposure period.

The equation of $x_{e(0.95)}$ (described in Chapter 4) were obtained for alloys 3003, 5049, and 6063, given in Table 6.1.

Alloy type	Extrapolated Equation
3003	$x_{e(0.95)} = 118t + 77.7$
5049	$x_{e(0.95)} = 6.3t - 3$
6063	$x_{e(0.95)} = 308.6 ln\,(t) - 69.1$

Table 6.1: Calculated equations for life time prediction.

For instance, a tube of alloy 5049 with thickness $5\,cm$ exposed to the sea water will be penetrated approximately (5% probability) after 21.7 years and a pit with 5cm in depth will be occur at a tube of alloy 3003 in the same condition after 1.16 years. It is important to stress that current discussion is based on simple fitting to the curve of distribution parameters as a function of time. Using more accurate method is suggested by author. Moreover, the solution used in SWAAT test was acidified seawater according with with ASTM D1141 that is more aggressive than natural seawater and higher temperature was applied during test duration. It is stated in many articles [68, 76, 78] that temperature has a significant influence on corrosion of aluminium alloys.

Chapter 7

Conclusion and further work

7.1 Concluding remarks

In this work, corrosion behaviour of four types of Al alloy were evaluated through electrochemical measurements and salt spray test. Then, statistical analysis of pit depth data was performed using the extreme value theory. Following conclusions can be drawn from the results.

- The corrosion behaviour of alloys 3003, 5049, 6061, and 6063 were found to be linked to the chemical composition and microstructure. The OCP measurements showed that alloy 3003 corrodes at more positive potential in both NaCl and SWAAT solutions due to high amount of Mn content. The more negative OCP for alloy 5049, 6061, and 6063 was observed which is connected with the Mg content of these alloys.

- There is not a significant difference between OCP of alloy 5049 and 6xxx (which were studied in this project) that can be connected to the low amount of Mn and higher amount of Mg in these alloys comparing with 3003.

- Alloy 5049 exhibited extensive passive region and low corrosion current density that demonstrates high corrosion resistance of this alloy. Alloy 3003 indicated very high corrosion current density and very short passive region that means this alloy has low corrosion resistance in the NaCl solution.

- The salt spray test showed alloy 3003 corrodes with relatively high corrosion rate. In addition to pitting, intergranular corrosion was observed in alloy 3003 due to presence of Cu content. Among studied alloys, alloy 5049 has the lowest corrosion rate. The second resistant alloy was alloy 6061.

- For all the alloys under study, potentiodynamic polarization results were in agreement with the corrosion test results. Generally, Mg content increases the ability of forming the passive film on the surface causing high corrosion resistance in synthetic seawater solution. On the other hand, Cu and Fe containing particles in microstructure decrease the corrosion resistance of the alloys.

- The Gumbel extreme value distribution fitted successfully to the data obtained for alloys 3003, 5049 and 6063 exposed to acidified seawater solution. The Gumbel distribution is a useful model for predicting the lifetime of a component made of these alloys exposed to seawater.

- For alloy 6061, full probability distribution of extreme pit depth is bi-modal for longer exposure, with the Gumbel distribution for smaller pits and another distribution, probably the Normal distribution, for deeper pits.

7.2   Topics for further research

Extended experimental

- In order to study the effect of microstructure on corrosion behaviour, the nature and distribution of second phase particles plays and important role. It is highly suggested to carry out a research based on SEM and EDS analysis to study the effect of second particles on corrosion resistance and pit growth.

- Heat treatment has a significant effect on second phases character and distribution in aluminium alloys. Performing a research on the effect of heat treatment on corrosion behaviour of Al alloys will demonstrate valuable result.

- Regarding statistical analysis, it is worth to generate more data to plot the maximum pit distribution more accurately. Thus, increasing the number of samples will help to plot better fit.

Extended statistical analysis

- Graphical method was used in this project to calculate the scale and location parameters of Gumbel plot. It is recommended to use other methods such as Likelihood or computer base models to estimate the parameters. It is also valuable to compare obtained result from graphical method with other methods to decide which method is appropriate.

Bibliography

[1] Z. Szklarska-Smialowska, "Pitting corrosion of aluminuim," *Corrosion Science*, vol. 41, pp. 1743–1767, 1999.

[2] R. Davis, *Corrosion of Aluminum and Aluminum Alloys*. ASM International, 1999.

[3] W. S. Tait, "Effect of physical parameters on the pitting corrosion of mild steel in low total dissolved solids, oxygen bearing waters: A nonpassivating metal/environment system," *Corrosion*, vol. 35, no. 7, pp. 296–300, 1979.

[4] Z. Ahmad, A. Ul-Hamid, and B. Abdul-Aleem, "The corrosion behavior of scandium alloyed al 5052 in neutral sodium chloride solution," *Corrosion Science*, vol. 43, no. 7, pp. $1227 - 1243$, 2001.

[5] B. Zaid and D. S. S. Benziad, "Effects of pH and chloride concentration on pitting corrosion of AA6061 aluminum alloy," *Corrosion Science*, vol. 50, 2008.

[6] Y. Liu, G. Meng, and Y. Cheng, "Electronic structure and pitting behavior of 3003 aluminum alloy passivated under various conditions," *Electrochimica Acta*, vol. 54, 2009.

[7] W. Liang, P. Rometsch, L. Cao, and N. Birbilis, "General aspects related to the corrosion of 6xxx series aluminium alloys: Exploring the influence of Mg/Si ratio and Cu," *Corrosion Science*, vol. 76, pp. $119 - 128$, 2013.

[8] R. Buchheit, "A compilation of corrosion potentials reported for intermetallic phases in aluminum alloys," *Journal of the Electrochemical Society*, vol. 142, 1995.

[9] M. Zamin, "The role of Mn in the corrosion behavior of Al-Mn alloys," *Corrosion*, vol. 37, 1981.

[10] K. A. Yasakau, M. L., Zheludkevich, S. V., and L. M. G. Ferreira, "Role of intermetallic phases in localized corrosion of aa5083," *Electrochimica Acta*, vol. 52, pp. 7651–7659, 2007.

[11] R. Melchers, "Extreme value statistics and long-term marine pitting corrosion of steel," *Probabilistic Engineering Mechanics*, vol. 23, 2008.

[12] V. S. Sinyavskii and V. D. Kalinin, "Marine corrosion and protection of aluminum alloys according to their composition and structure," *Protection of Metals*, vol. 41, pp. 317–328, 2005.

[13] N. Laycock, P. Laycock, P. Scarf, and D. Krouse, "Applications of statistical analysis techniques in corrosion experimentation, testing, inspection and monitoring," 2010.

[14] P. Aziz, "Application of the statistical theory of extreme values to the analysis of maximum pit depth data for aluminum," *Corrosion*, vol. 13, pp. 495–506, 1956.

[15] J. Vajo, R. Wei, A. Phelps, L. Reiner, G. Herrera, O. Cervantes, D. Gidanian, B. Bavarian, and C. Kappes, "Application of extreme value analysis to crevice corrosion," *Corrosion Science*, vol. 45, pp. 497–509, 2003.

[16] P. Sheasby and R. Pinner, *The surface treatment of aluminium and its alloys*, vol. 1. Finishing Publications Ltd., 2001.

[17] I. Polmear, "Metallurgy of the light metals," *Journal of Light Metals*, 1995.

[18] F. Mazzolani, *Aluminium alloy structure*. London: EFN Spon, 1995.

[19] P. Roberge, *Handbook of corrosion engineering*. New York: McGraw-Hill, 2000.

[20] G. Scamans and N. B. B. Buchheit, "Corrosion of aluminum and its alloys," *Elsevier Science*, 2010.

[21] C. Vargel, "Corrosion of aluminium," *Elsevier*, 2004.

[22] F. Lockwood, "Pitting corrosion of 5052 aluminuim alloy," *Applications of Surface Science*, vol. 20, pp. 339–346, 1985.

[23] J. R. Davies, *Corrosion of aluminium and aluminium alloys*. ASM International: MAterials Park, 1999.

[24] M. Keddam, C. Kuntz, H. Takenouti, D. Schuster, and Z. D., "Exfoliation corrosion of aluminium alloys examined by electrode impedance," *Electrochimica Acta*, vol. 42, pp. 87–97, 1997.

[25] M. Bocher F. Flower and M. Ryan, "The effect of microstructure on localized corrosion in creep age-formable aluminium alloys: identification of intermetallic particles and pit initiation sites," *Journal of Electrochemical Society*, vol. 153, 2006.

[26] G. J.R. and D. Micheli, "Mechanism of intergranular corrosion of Al-Cu alloys," *Corrosion Science*, vol. 10, 1970.

[27] E. Lee and S. Pyun, "The effect of oxide chemistry on the passivity of aluminium surfaces," *Corrosion Science*, vol. 37, no. 1, pp. $157 - 168$, 1995.

[28] V. Guillaumin and G. Mankowski, "Localized corrosion of 6056 T6 aluminium alloy in chloride media," *Corrosion Science*, vol. 42, 2000.

[29] P. Rometsch, L. Cao, X. Xiong, and B. Muddle, "Atom probe analysis of early-stage strengthening behaviour in an Al-Mg-Si-Cu alloy," *Ultramicroscopy*, vol. 111, no. 6, pp. $690 - 694$, 2011. Special Issue: 52nd International Field Emission Symposium.

[30] D. Macdonald, H. Song, K. Makela, and K. Yoshida, "Corrosion potential measurements on type 304 ss and alloy 182 in simulated bwr environments," *Corrosion*, vol. 49, p. 8, 1993.

[31] J. Lyndon, R. Gupta, M. Gisbon, and N. Birbilis, "Electrochemical behaviour of the beta phase intermetallic as a function of pH as relevant to corrosion of AlMg alloys," *Corrosion Science*, vol. 70, 2013.

[32] Q. Meng and G. S. Frankel, "Effect of cu content on corrosion behavior of 7xxx series aluminum alloys," *Journal of The Electrochemical Society*, vol. 151, 2004.

[33] O. Seri and M. Imaizumi, "The dissolution of FeAl3 intermetallic compound and deposition on aluminum in AlCl3 solution," *Corrosion Science*, vol. 30, no. 11, pp. $1121 - 1133$, 1990.

[34] R. A., J. Davenport, M. Scamans, and A. Afseth, "Effect of iron-containing intermetallic particles on the corrosion behaviour of aluminium," *Corrosion Science*, vol. 48, no. 11, pp. $3455 - 3471$, 2006.

[35] Z. Szklarska-Smialowska, "Pitting corrosion of aluminum," *Corrosion Science*, vol. 41, pp. 1743–1767, 1999.

[36] I. L. Muller and J. Galvvele, "Pitting potential of high purity binary aluminum alloys- AlMg and AlZn alloys," *Corrosion Science*, vol. 17, pp. 995–1007, 1977.

[37] S. Ringer and K. Hono, "Nucleation of precipitates in aged AlCuMg(Ag) alloys with high Cu:Mg ratios," *Acta Materialia*, vol. 44, pp. 1883–1898, 1996.

[38] R. Buchheit and P. Grant, "Local dissolution phenomena associated with S phase particles in aluminum alloy 2024-T3," *Journal of theElectrochemical Society*, vol. 144, pp. 2621–2628, 1997.

[39] W. Miao and D. Laughlin, "Effects of Cu content and preaging on precipitation characteristics in aluminum alloy 6022," *Metallurgical and Materials Transactions*, vol. 31, 2000.

[40] K. Yasakau, M. Zheludkevich, S. Lamaka, and M. Ferreira, "Role of intermetallic phases in localized corrosion of AA 5083," *Electrochimica Acta*, vol. 52, p. 7651, 2007.

[41] C. B. Kuhla, *Application of Extreme Value theory in the reliability analysis of non-electronic components*. PhD thesis, School of Engineering, 1967.

[42] R. Melchers, "Statical characterization of pitting corrosion-part 1: data analysis," *Corrosion Science*, vol. 61, p. 655, 2005.

[43] P. Lay, P. L. Cottis, and A. Scarf, "Extrapolation of extreme pit depths in space and time," *Journal of Electrochemical Society*, vol. 137, no. 1, 1990.

[44] "Corrosion of metals and alloys- guidelines for applying statistics to analysis of corrosion data," 2012.

[45] K. M., "Introduction to life prediction of industrial materials: Application of the extreme value statistical method for corrosion analysis," *Allerton Press*, 1994.

[46] T. Shibata, "Application of extreme value statistics to corrosion," *Journal of Research of the National Institute of Standards and Technoloy*, vol. 99, p. 327, 1994.

[47] J. Strutt, J. Nicholls, and B. Barbier, "The prediction of corrosion by statistical analysis of corrosion profiles," *Corrosion Science*, vol. 5, 1985.

[48] S. Coles, "An introduction to statistical modeling of extreme values," *Springer Series in Statistics*, 2001.

[49] T. Summerson, M. Pryor, and R. Hogan, *Pit depth measurements as a means of evaluating the corrosion resistance of aluminium in seawater*. In Special Technical Publication, 1957.

[50] D. Rivas, F. Caleyo, A. V. b., and J. Hallen, "Extreme value analysis applied to pitting corrosion experiments in low carbon steel: Comparison of block maxima and peak over threshold approaches," *Corrosion Science*, vol. 50, 2008.

[51] Y. Fukuda and H. Kawasaki, "Statical analysis of pitting corrosion of heat exchanger tubes," *58th Corrosion and Protection Symposium*, p. 24, 1984.

[52] *Standard Guide for Examination and Evaluation of Pitting Corrosion*. No. G46-94, ASTM International, 2005.

[53] A. Fougeres, S. Holm, and H. Rootzen, "Pitting corrosion: Comparison of ttreatment with extreme value distributed responses." Report by Volvo Car Company.

[54] J. Nicholls and D. Stephenson, "A life prediction model for coatings based on the statistical analysis of hot salt corrosion performance," *Corrosion Science*, vol. 33, no. 8, pp. 1313 − 1325, 1992.

[55] J. Strutt, J. Nicholls, and B. Barbier, "The prediction of corrosion by statistical analysis of corrosion profiles," *Corrosion Science*, vol. 25, no. 5, pp. 305 − 315, 1985.

[56] E. Castillo, A. Hadi, N. Balakrishnan, and J. Sarbia, *Extreme Value and Related Models with Applications in Engineering and Science*. New Jersey: John Wiley, 2005.

[57] R. E. Melchers, "Representation of uncertainty in maximum depth of marine corrosion pits," *Structural Safety*, vol. 27, pp. 322–334, 2005.

[58] J. Silva, A. Bustamante, E. Codaro, R. Nakazato, and L. Hein, "Morphological analysis of pits formed on Al 2024-T3 in chloride aqueous solution," *Applied Surface Science*, vol. 236, pp. 356 − 365, 2004.

[59] M. Bethencourt, F. Botana, M. Cano, M. Marcos, J. Sanchez-Amaya, and L. Gonzalez-Rovira, "Behaviour of the alloy AA2017 in aqueous solutions of NaCl. part i: Corrosion mechanisms," *Corrosion Science*, vol. 51, no. 3, pp. 518 − 524, 2009.

[60] S. Li, H. Zhang, and J. L. Liu, "Corrosion behavior of aluminum alloy 2024-T3 by 8-hydroxy-quinoline and its derivative in 3.5 percent chloride solution," *Transactions of Nonferrous Metals Society of China*, vol. 17, no. 2, pp. 318 − 325, 2007.

[61] H. Allachi, F. Chaouket, and K. Draoui, "Corrosion inhibition of AA6060 aluminium alloy by lanthanide salts in chloride solution," *Journal of Alloys and Compounds*, vol. 475, pp. 300 − 303, 2009.

[62] H. P. Godard and W. B. Jepson, *The Corrosion of Light Metals*. Wiely, 1967.

[63] B. Zaid, D. Saidi, A. Benzaid, and S. Hadji, "Effects of pH and chloride concentration on pitting corrosion of AA6061 aluminum alloy," *Corrosion Science*, vol. 50, p. 1841, 2008.

[64] N. Belov, *Iron in Aluminum Alloys*. Taylor and Francis Inc., 2002.

[65] N. Liu, J. Wang, L. Wang, Y. Wu, and L. Wang, "Electrochemical corrosion behavior of Al-Mg-Nd in NaCl solution," *Corrosion Science*, vol. 51, no. 6, pp. 1328 − 1333, 2009.

[66] H. Olsen, A. Afseth, and K. Nisancioglu, "Filiform corrosion of aluminium sheet, electrochemical and corrosion behaviour of bare substrates," *Corrosion Science*, vol. 40, 1998.

[67] A. Afseth, J. H. Nordlien, G. M. Scamans, and K. Nisancioglu, "where there is difficulty of obtaining meaningful data due to the dynamic nature of such surfaces," *Corrosion science*, vol. 44, pp. 2491–2506, 2002.

[68] B. Brown, J. Kruger, and R. Siahle, "Critical ppotential for localized corrosion of aluminum alloys," *National Assosiation of Corrosion Engineering*, p. 580, 1974.

[69] G. Svenningsen, M. Larsen, J. C. Walmsley, J. H. Nordlien, and K. Nisancioglu, "Effect of artificial aging on intergranular corrosion of extruded AlMgSi alloy with small Cu content," *Corrosion Science*, vol. 48, no. 6, pp. 1528 − 1543, 2006.

[70] H. Godard, W. Jepsen, and M. Bothwell, *The Corrosion of Light Metals*. New York: John Wiley and Sons, 1967.

[71] G. Burstein, C. Liu, R. Souto, and S. Vines, "Origins of pitting corr," *Corrosion E*, vol. 39, pp. 25–30, 2004.

[72] P. Marcus, *Corrosion Mechanisms in Theory and Practice*. New York: Marcel Dekker, 2002.

[73] R. Melchers, "Pitting corrosion of mild steel under marine anaerobic conditions- part 1: experimental observations," *Corrosion*, vol. 62, pp. 981–988, 2006.

[74] J. Strutt, J. Nicholls, and B. Barbier, "The prediction of corrosion by statistical nanalysis of corrosion profiles," *Corrosion Science*, vol. 5, pp. 305–315, 1985.

[75] R. E. Melchers, "Extreme value statistics and long-term marine pitting corrosion of steel," *Probabilistic Engineering Mechanics*, vol. 23, pp. 482–488, 2008.

[76] R. W. Revie, *Oil and Gas Pipelines: Integrity and Safety Handbook*. John Wiley and Sons, 2015.

[77] D. Frangopol and J. D. Sorensen, *Advances in Reliability and Optimization of Structural Systems*. CRC Press, 2005.

[78] R. T. Foley, "Localized corrosion of aluminum alloys-review," *Corrosion*, vol. 42, no. 5, pp. 277–288, 1986.

Appendix

A   Pit depth measurements

The 10 deepest pit on each sample were selected and pit depth was measured using optical microscopy. Tables 7.2-7.3, present the whole data set for all alloys.

Exposure period (day)	Pit 1	Pit 2	Pit 3	Pit 4	Pit 5	Pit 6	Pit 7	Pit 8	Pit 9	Pit 10
2	10						28			
2	53	10	30	21	38	18				
6	23	30	24	15	15	25	21	62		
6	18	22	24	14	20	17	29	22		
10	16	26	35	14	29	20	24	33	21	28
10	15	44	22	14	10	11	22	14	20	21
13	10	16	25	24	25	17	8	27	10	38
13	28	12	23	12	32	48	22	30	18	11
17	29	17	22	35	27	30	41	27	23	42
17	20	26	22	16	34	17	48	10	36	16
21	60	85	105	53	10	56	33	35	30	40
21	134	26	52	48	43	24	52	28	35	34
24	52	94	120	112	76	31	44	69	72	89
24	47	52	38	67	50	87	54	81	96	30
28	38	40	60	36	42	37	35	46	35	22
28	54	43	50	64	76	42	55	123	40	62
34	105	84	83	50	128	93	54	89	62	92
34	38	93	48	56	63	51	42	16	323	295
38	83	86	76	35	53	240	42	51	52	74
38	70	87	140	30	51	54	60	45	62	71
45	82	85	64	86	70	40	120	54	62	75
45	95	105	265	20	230	73	160	83	52	70
49	35	66	130	57	90	78	50	35	64	73
49	96	134	60	40	163	30	290	95	152	53

Table 7.1: Pit depth data for alloy 5049. Measurements are in μm.

Exposure period (day)	Pit 1	Pit 2	Pit 3	Pit 4	Pit 5	Pit 6	Pit 7	Pit 8	Pit 9	Pit 10
1	5	10				6	92	75	28	112
1	18	13	8	160	14	24	9	15		
2	166	97	190	90	42	157	96	112	128	200
2	250	84	94	105	144	185	95	90	10	148
3	101	358	155	195	381	120	107	42	35	82
3	310	110	195	62	140	75	262	283	150	182
6	593	680	500	375	540	200	444	540	535	335
6	272	350	445	453	280	380	583	421	206	405
7	637	512	147	276	415	281	360	575	612	540
7	526	609	674	503	341	444	423	598	500	574
10	820	658	642	759	673	553	843	795	727	515
10	1045	1040	977	815	645	693	758	598	752	1016

Table 7.2: Pit depth data for alloy 3003. Measurements are in μm.

Exposure period (day)	Pit 1	Pit 2	Pit 3	Pit 4	Pit 5	Pit 6	Pit 7	Pit 8	Pit 9	Pit 10
2	10	5	40	68	56					
2	7	10	14	17	58	53	10			
6	368	209	242	206	371	400	405	352	262	394
6	262	272	317	407	330	357	369	357	277	478
10	287	364	556	546	295	420	448	185	410	437
10	360	244	427	343	213	587	476	172	368	250
13	358	322	432	250	363	454	413	591	218	371
13	585	645	296	667	601	337	438	445	475	470
17	457	365	518	545	454	537	502	413	240	578
17	475	343	285	711	432	738	392	495	410	511
21	118	432	583	710	494	467	426	616	460	347
21	608	670	543	636	745	560	518	488	530	475
24	607	850	710	735	844	462	527	537	770	704
24	592	663	567	440	660	528	636	590	505	420
28	520	637	620	375	610	715	474	765	600	620
28	547	356	768	580	460	610	490	423	575	585

Table 7.3: Pit depth data for alloy 6063. Measurements are in μm.

Exposure period (day)	Pit 1	Pit 2	Pit 3	Pit 4	Pit 5	Pit 6	Pit 7	Pit 8	Pit 9	Pit 10
2	9	22	61	14	12					
2	72	42		17	90	114				
6	421	363	300	457	354	181	331'	398	205	445
6	217	359	330	244	298	373	440	260	197	67
10	363	243	420	460	280	216	252	437	253	360
10	249	447	257	362	507	400	635	398	410	376
13	478	498	433	285	558	456	457	600	492	543
13	327	260	334	277	405	421	337	358	327	291
17	229	577	515	580	375	607	730	445	550	270
17	540	534	255	625	687	562	660	690	595	588
21	1052	703	347	537	863	520	568	546	475	255
21	395	420	404	250	436	320	353	425	517	256
24	500	417	505	664	475	695	246	157	459	243
24	443	925	270	354	440	495	300	533	565	450
28	680	653	694	415	876	656	378	443	507	500
28	562	442	469	475	590	478	485	650	577	550
34	670	766	532	720	503	740	762	557	480	466
34	628	480	780	385	600	535	720	560	410	550
38	910	888	1010	890	624	480	878	630	550	527
38	815	486	384	1076	636	720	340	532	620	617
45	354	734	710	430	362	438	415	557	368	505
45	662	690	360	873	1037	560	625	595	446	573
49	320	645	790	810	560	670	763	745	825	620
49	675	800	630	550	590	757	690	1020	585	624

Table 7.4: Pit depth data for alloy 6061. Measurements are in μm.

B Pit morphology

(a) 2 days

(b) 6 days

(c) 7 days

(d) 10 days
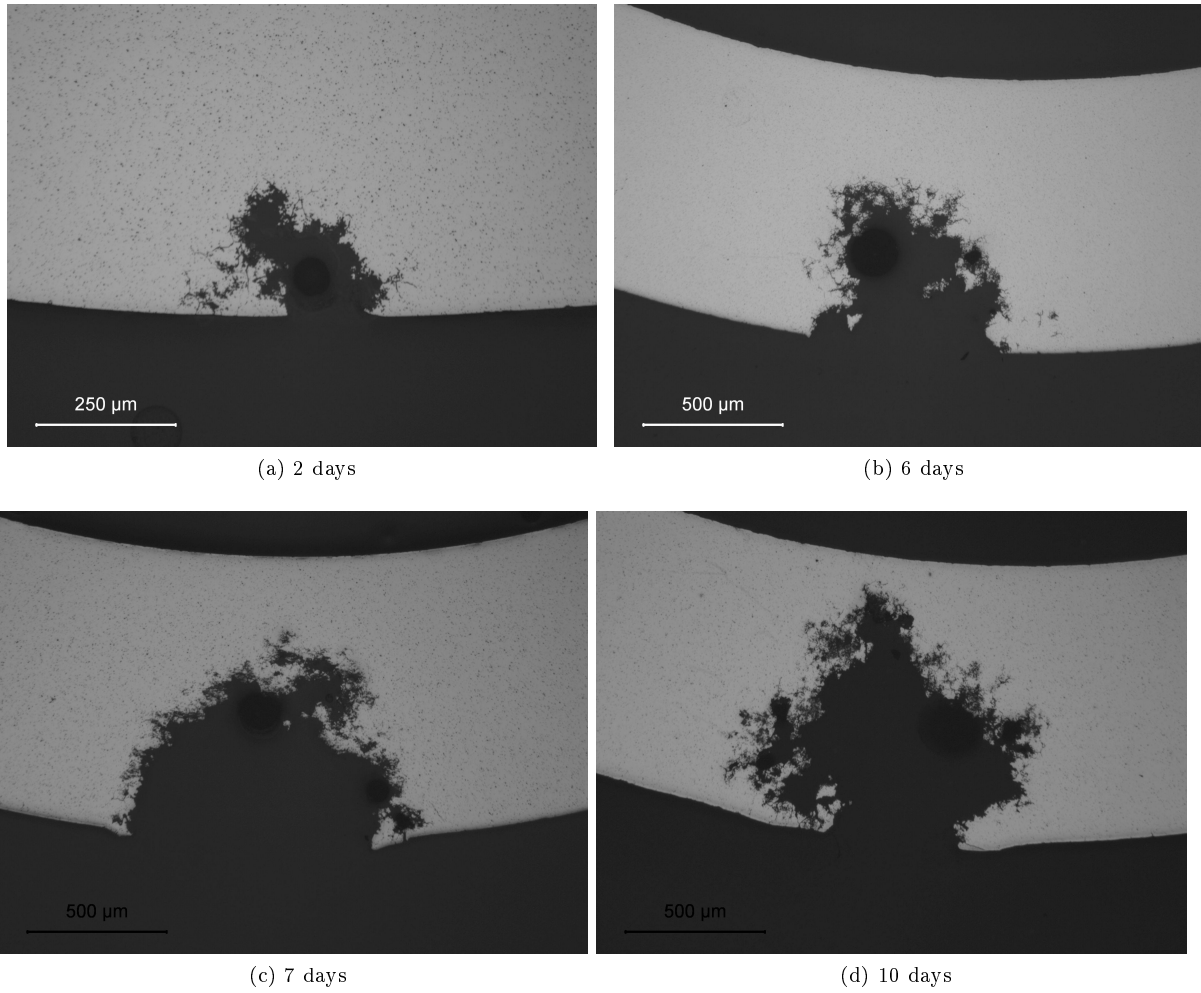
Figure 7.1: Pit morphology of alloy 3003 after different exposure periods.
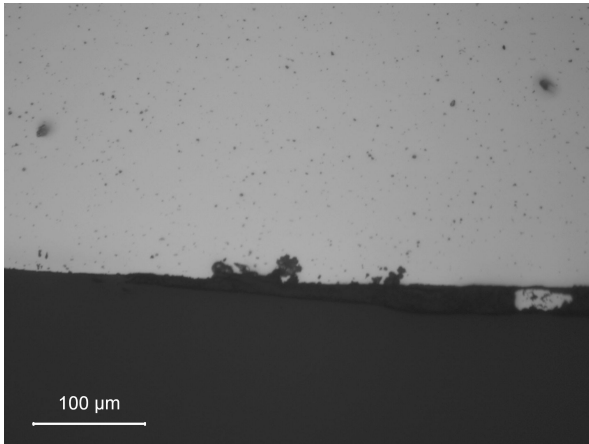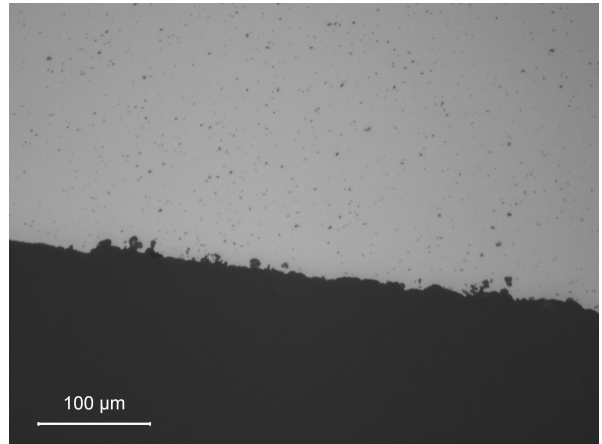
(a) 13 days

(b) 17 days
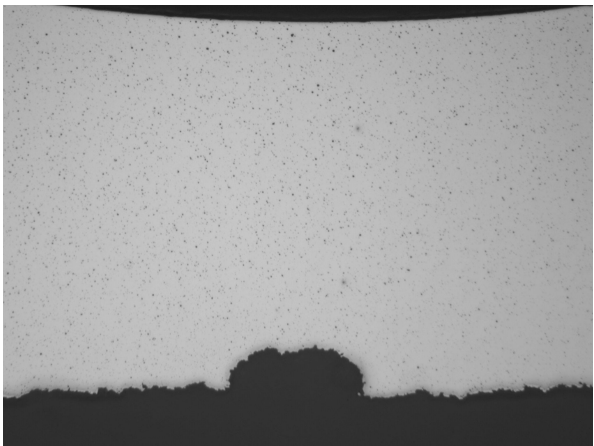
(c) 34 days
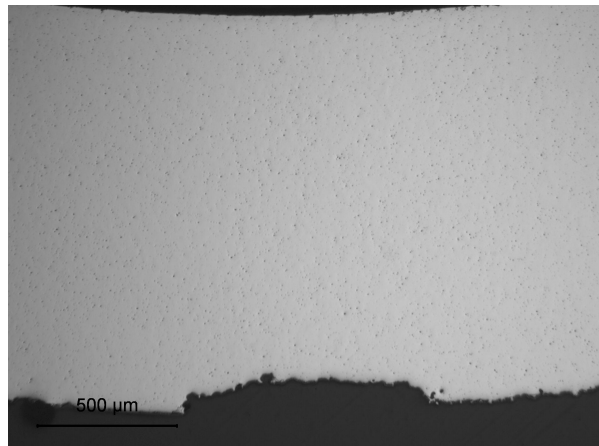
(d) 49 days

Figure 7.2: Pit morphology of alloy 5049 after different exposure periods.
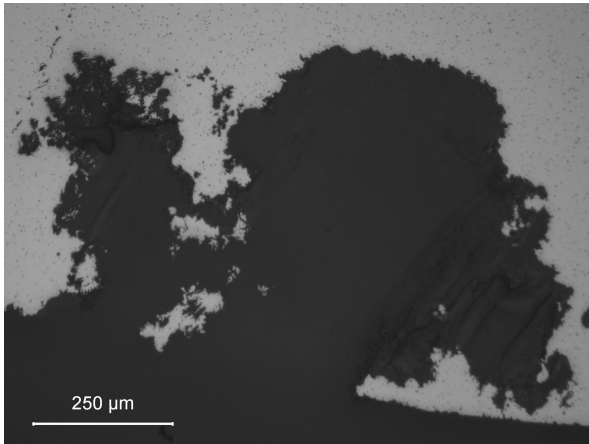
(a) 13 days
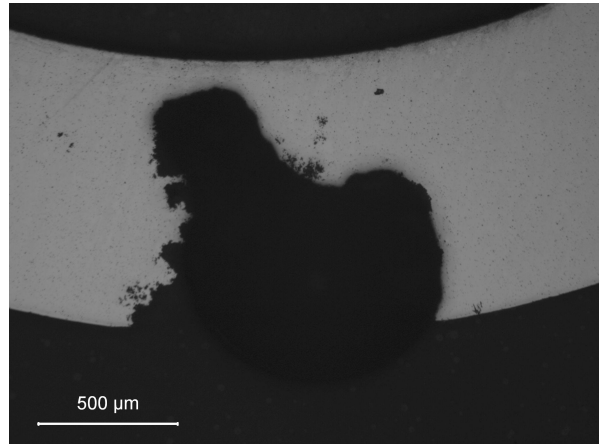
(b) 21 days
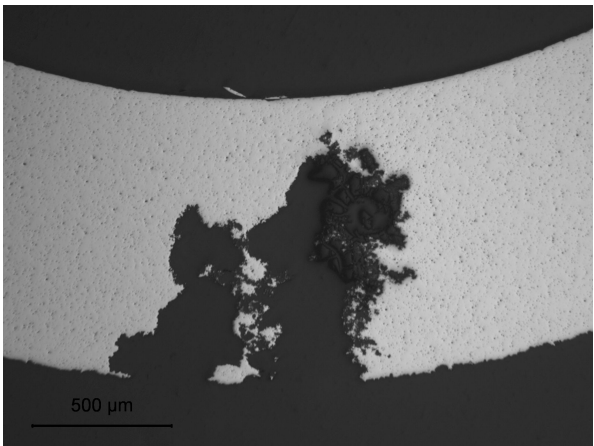
(c) 28 days
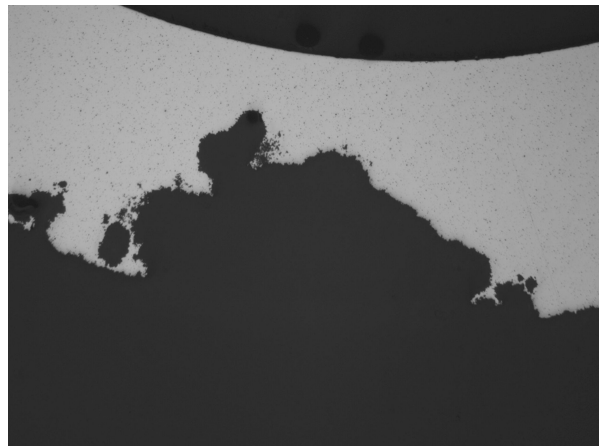
(d) 45 days

Figure 7.3: Pit morphology of alloy 6061 after different exposure periods.
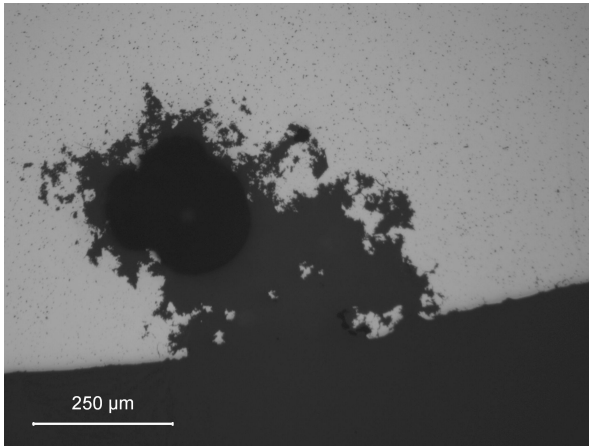
(a) 6 days
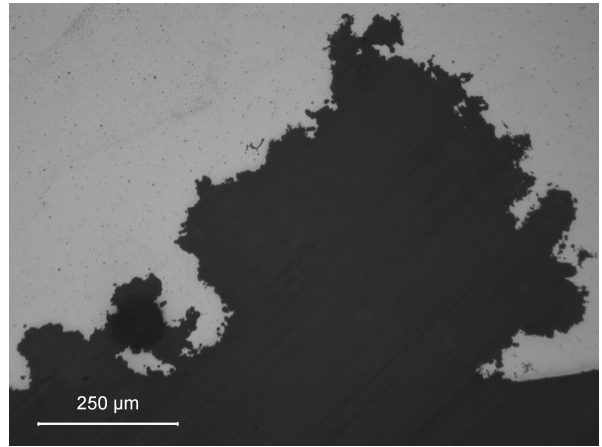
(b) 17 days
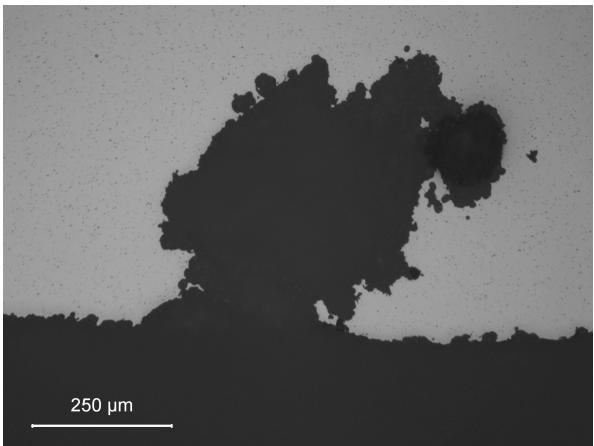
(c) 21 days
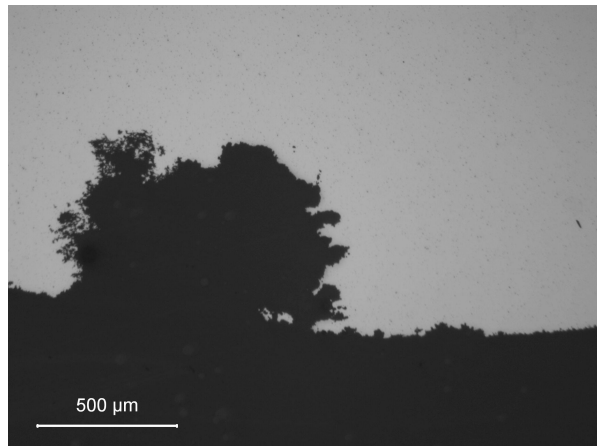
(d) 28 days

Figure 7.4: Pit morphology of alloy 6063 after different exposure periods.